THE EFFECTS OF FEMTOSECOND LASER CREATED DRAINAGE CHANNELS ON THE AQUEOUS HUMOR OUTFLOW DYNAMICS OF THE EYE

by

Dongyul Chai

A dissertation submitted in partial fulfillment
of the requirements for the degree of
Doctor of Philosophy
(Biomedical Engineering)
in The University of Michigan
2008

Doctoral Committee:

Associate Professor Alan J. Hunt, Co-Chair
Professor Tibor Juhasz, The University of California, Irvine, Co-Chair
Professor Theodore B. Norris
Associate Professor Joseph L. Bull
Assistant Research Scientist Kyle W. Hollman
Professor Matthew O'Donnell, The University of Washington

To My Parents

ACKNOWLEDGEMENTS

Looking back over my life for last eight years, I have been very fortunate that I could be with great people and get a lot of help from them. Most of all, I would like to take this opportunity to thank my family, especially my parents, for their consistent support throughout my life. Whenever I was depressed or experiencing difficulty, they encouraged me to never give up and to always keep going. I would have not even started studying abroad without their support and encouragement.

I would like to thank Dr. Tibor Juhasz, my advisor, for giving me the chance to start my research career. He helped me to improve myself by developing my abilities to identify and solve the problem at hand. I learned from him the attitude towards work and the significance of work ethic and diligence. I could also get the valuable experience of building the lab from the initial stage.

I would like to appreciate Dr. Matt O'Donnell, my co-advisor, currently in the University of Washington. I got a lot of help from him for the whole process of the PhD program. Specifically, with his support I could continue and finish my PhD program through the hard process during which the lab was moved into California. I also thank Dr. Alan Hunt in the University of Michigan, co-chair of the committee, for his help to complete the program, working in the University of California at Irvine.

I will not forget the help from Dr. Ron Kurtz of the University of California at Irvine. His advice based on medical, clinical knowledge was a huge asset to complete my research and keep it going in the right direction.

Considering that no research can be done without help or cooperation with colleagues, I am very grateful for the help of my research colleagues, Gautam Chaudhdary, Eric Mikula and Hui Sun in our lab, and research colleagues at the Laser Institute and the Eye Research Center. Their effort and knowledge of the research helped me to make progresses in my research and complete my PhD work from experimenting to modeling.

I can not forget the help and support from my friends and seniors. I thank Hyungson Ki, a professor in Michigan State University, for his personal mentoring of my life. He has given me the insightful advice on everything in my life since I met him in June 2000. I also give thanks to another personal mentor, Minkyung Song, currently a professor in Kyonggi University in Korea, for her continuous mentoring over every aspect of my life. I also got a lot of help from Sukyung Park, a professor in Korea Advanced Institute of Science and Technology. I thank to Sung-joon Hwang, Moonbin Yim, Juseop Lee, Hyunjin Lim and Sungwook Lee and other seniors and friends for their help and support in US and Tae-Jung Kim, Phil-Soo Kim, Jinhong Min and Dohyun Kim in Korea. I appreciate Professor Seung-Hyun Yoo of Ajou University in Korea for his continuous help and support.

TABLE OF CONTENTS

LIST OF FIGURES

ABSTRACT

THE EFFECTS OF FEMTOSECOND LASER CREATED DRAINAGE CHANNELS ON THE AQUEOUS HUMOR OUTFLOW DYNAMICS OF THE EYE

by

Dongyul Chai

Co-Chairs: Alan J. Hunt and Tibor Juhasz

Various treatments have been introduced to delay or slow the progress of glaucoma, one of the leading causes of blindness, by reducing intraocular pressure (IOP), the unique manageable factor in glaucoma. However, there are limitations to the continuous usage of currently available treatments. A femtosecond laser presents the potential of advanced treatment by significantly reducing damage to tissues. This dissertation will address the compressive aspects of glaucoma and its treatments and the development of a minimally invasive surgical procedure and a supporting tool to improve the efficiency of this procedure.

The experimental setup was built to scan the eye with a femtosecond laser in a predetermined pattern with adjustable parameters. The outflow rate was measured before and after the laser treatment to evaluate the effect of the channel. It was demonstrated that the subsurface scleral channel that increases aqueous humor (AH) outflow rate can be created in *ex vivo* rabbit eyes with a femtosecond laser.

Considering that the goal of glaucoma treatment is to reduce IOP into the normal range, a tool is required to predict the channel dimensions to achieve a predetermined IOP reduction. I developed a 3D finite element model and demonstrated its potential as a tool for estimating channel dimensions by fitting the experimental data to the model.

The experimental setup was altered to make a scan on an *in vivo* rabbit. It was demonstrated that the subsurface scleral channel can be created in the eyes of *in vivo* rabbits and IOP can be reduced with this channel. It was found that IOP can be reduced with a positive relation to the dimensions of the channel, demonstrating the potential for controlled IOP reduction by manipulating channel dimensions.

Therefore, it can be concluded that the subsurface scleral AH drainage channel can be created with a femtosecond laser, overcoming the disadvantages of current treatments. The method has the potential of controlling IOP reduction with the channel dimensions. 3D FEM has potential as a tool for predicting the post treatment IOP and calculating channel dimensions for a required IOP reduction.

CHAPTER 1

INTRODUCTION

1.1. Chapter Outline

Glaucoma is a progressive eye disease. Therefore, the understanding of fundamentals of the structure and physiology of the eye should provide the insight into glaucoma from cause, effect to the way it can be treated. In section 1.2, the overall structure of the eye, the role of each part and the mechanism of the vision is reviewed. Glaucoma occurs due to change in properties of some parts. Therefore, the details of property changes causing glaucoma and the process glaucoma can occur, progress and effect of the vision will be elaborated also.

The primary cause for glaucoma is changes in properties of some parts of the eye. Therefore, the glaucoma treatment is to return the changed properties to the original ones or make adjustment so that effects of property changes can be eliminated. In section 1.3, the mechanism of treating glaucoma, the way of classifying the glaucoma treatments will be introduced. The merits and demerits of each treatment will be also discussed providing the insight into the optimal treatment and how it will be developed.

Lasers were introduced to the eye treatment in an effort to overcome the disadvantage of other treatments with very reduced and localized damage caused by this technology. In section 1.4, the last section of this chapter, the brief history of applying a laser to the surgical treatment and the fundamentals of laser tissue interaction will be introduced focused on the mechanisms the energy of laser beam can be deposited into the tissue. The history of development by introducing various lasers is provided. It will be also elaborated which effects each parameter has on improving the quality of treatments, indicating directions for future developments.

1.2. Structure and Physiology of the Eye

1.2.1. Overall Structure of the Eye

The basic structure of the eye is shown in Figure 1.1. Entering light is refracted by the cornea and lens to form an image on the retina. Lens thickness is adjusted by the zonules to form a sharp image on the retina, which is evident at the fovea. [1]. The interior of the eye is composed of the anterior chamber, posterior chamber, and vitreous chamber, as described in Figure 1.1 and Figure 1.2.

1.2.2. Anterior Chamber

As it can be seen in Figure 1.2, the anterior chamber is the space roofed by the cornea and floored by the lens and iris whose root is surrounded by trabecular meshwork. The cornea is connected to the sclera through the Schwalbe's line, which is the limit of corneal endothelium. Limbus is the intermediate zone of connective tissues between cornea and sclera [2].

The cornea, the most anterior part of the eye, is the clear vascular structure providing a clear refractive interface, tensile strength, and protection from external factors [3]. The cornea is also can be modeled as a viscoelastic material when it is stretched and has no channel allowing bulk flow [1]. Anatomically, the cornea is composed of five layers, from the anterior layer, epithelium, Bowman's membrane, stroma, Descemet's membrane, and endothelium [1]. Its light transparency is from the stroma, an organized arrangement of collagen fibrils [4].

The lens plays an accommodating role to make light focus on the retina [2]. It is composed of concentric layers defining the nucleus and cortex, with epithelial cells at the anterior surface and a capsule at the posterior part [5]. Lens volume is not appreciably affected by new fibers laid down with time, but the lens becomes harder over time and it becomes more difficult to accommodate the shape with zonules, leading to damage of the sharp image on retina [4].

The iris controls the amount of light allowed through the lens by adjusting the diameter of the pupil. It adjusts its length by the contraction and dilation of posterior and anterior leaves using blood vessels and nerves [6]. These vessels provide the heat driving AH flow toward the cornea by convection.

The sclera is a structure defining five sixths of the outer surface of the eye [7]. It has distinct layers, including from the inside the lamina fusca in contact with the chroid, scleral stroma, episclera, and Tenon's capsule [7]. It also has a special structure on the posterior side called the lamina cribrosa where axons from the optic nerve exit the eye [7]. The sclera plays a significant role in protecting the eye and keeping optical stability with

its rigidity, maintaining the shape of the eye, movement of the eye, and defining the intraocular pressure (IOP) [7].

1.2.3. Posterior Chamber

The posterior chamber is the space defined by the posterior surface of the iris and the inner surface of the ciliary body, ciliary processes, lens, and zonules as shown in Figure 1.2. It is connected to the anterior chamber through the channel between the lens and iris. The ciliary processes is where AH is secreted as described below in the aqueous humor (AH) dynamics section. The zonules are composed of elastic fibers and their role is to stabilize and accommodate the lens. The fiber structure of zonules allows AH to flow into the vitreous [6].

1.2.4. Vitreous Chamber

The vitreous chamber is the space filled with vitreous humor, defined by the posterior surface of the lens, zonules, and the retina below the ciliary body as described in Figure 1.1 and Figure 1.2. Approximately 80% of the eye volume is occupied by the vitreous chamber [6]. Vitreous humor interacts with the retina, ciliary body, lens, and mechanically supports the structures it contacts [5]. There are fibrils in the vitreous humor with collagen banding, but about 99% of vitreous mass is water [5].

Light is detected at the retina by converting light energy into chemical energy in the photoreceptors [5]. Following detection, the brain recognizes the event by conveying the signal with bipolar and ganglion cells and finally converting it into action potentials, and ultimately, going down to the brain through the axon [5]. The retina is composed of ten layers from the outmost pigment epithelium to the inmost inner limiting membrane [5]. The fovea has the highest visual acuity, [1] and also has stronger pigmentation of the

pigment epithelium than other areas of retina, producing significant light suppression in this region. Photoreceptors are slender around the center of the fovea, increasing the density of photoreceptor. The increased number of receptors around the central fovea enhances visual acuity [1].

The choroid is the layer between the sclera and the retina with the largest blood flow such that problems in choroidal blood vessels are related to peripheral retinal degeneration [1]. The choroid nourishes the retina and removes the heat produced when light hits the retina. In addition, the choroid cushions the interior structure of the eye [1].

1.2.5. Aqueous Humor (AH) Dynamics

1.2.5.1. Aqueous Humor Formation

AH is produced from ciliary processes and exits the eye through pathways as described in Figure 1.2**.** AH maintains the refractive properties of the eye by maintaining IOP leading to the maintenance of cornea curvature [8]. AH also helps metabolic functions of avascular structures such as lens, cornea, and trabecular meshwork. AH provides nutrients like glucose and amino acids and removes wastes [9].

AH is produced from ciliary processes and secreted into the posterior chamber by diffusion, electrochemical gradient, and transport in exchange of chemical component like HCO^{3}- , H^{+} and [10, 11]. AH is composed of organic substances such as ascorbate, glucose and inorganic substances such as biocarnate, chloride, sodium [2]. The components playing noticeable roles in AH secretion have different concentrations depending on the locations as shown in Table. 1 [10]. Especially, Na^{+} and Cl^{-} have different concentrations between plasma inside ciliary body and anterior/posterior

chamber, backing up the existence of an active transport mechanism such as exchange pump and ion channel in the process of secreting AH into posterior chamber [10].

IOP is determined by AH dynamics, especially, the balance between inflow and outflow of AH to the anterior chamber. While circadian change of IOP is by the fluctuation of AH inflow [12], the elevation of IOP leading to glaucoma is by the alteration in the resistance of AH flow along outflow pathway [13]. Produced by ciliary processes, AH flows into the anterior chamber through the channel between the lens and the iris and exits the eye through two routes, trabecular (conventional) and uveoscleral (unconventional) pathways.

1.2.5.2. Trabecular (Conventional) Pathway

As it can be seen in Figure 1.3 and Figure 1.4, following the trabecular pathway, AH exits the eye through trabcular meshwork, Schlemm's canal, collector's channel, and to episcleral vein, its final destination of AH. The trabecular meshwork is composed of the uveal meshwork, corneoscleral meshwork, and juxtacanalicular meshwork [9]. Uveal meshwork has the porous structure with 25 – 75 μm diameter [14]. The diameter is reduced to be 2 – 15 μm in the deep layer of the corneoscleral meshwork [14]. It was proven experimentally that both of uveal and corneoscleral meshwork have ignorable outflow resistance [15].

The Juxtacanalicular meshwork (JCT) with 2–15 μm thickness [16] and 30–40% open space [14] is located between the corneoscleral meshwork and the Schlemms' canal, so that the inner endothelial layer is in contact with the corneoscleral meshwork and the outmost portion with inner wall of the Schlemm's canal [9]. JCT has been believed to be the source of majority of AH outflow resistance [16]. The Schlemm's canal is defined as

the space between the outer portions of juxtacanalicular meshwork composed of endothelial cells layer and the sclera [9]. The schlemm's canal is open at low IOP, but collapsed by the expanded trabecular meshwork at high IOP. The outflow resistance of canal at low IOP should be ignorable [18], but it is theoretically possible that the collapsed canal can provide the increased outflow resistance. However, it was found that IOP of non-glaucomatous eye can't be increased as high as glaucomatous eye by collapsing of the Schlemm's canal only [19, 20], leading to the conclusion that the collapse of Schlemm's canal can not cause glaucoma. Flowing out of Schlemm's canal, AH flows into the episcleral vein through collector's channel and the aqueous vein with tens of micrometer diameters [21]. It was demonstrated the outflow resistance in both are proved to be negligible [22] and it is supported by the experiments that the laser trabeculoplasty (LTP) acted on trabecular meshwork successfully reduced outflow resistance [23, 24]. Therefore, it can be concluded based on the studies that the most efficient way to reduce the outflow resistance along the trabecular pathway is to remove JCT. However, it should be very difficult to remove only the layer with 2–15 μm thickness inside the sclera.

1.2.5.3. Uveoscleral (Unconventiaonal) Pathway

As is described in Figure 1.2 and Figure 1.3, AH enters the uveoscleral pathway through ciliary muscle, flows across the ciliary body and exits through the supraciliary space and across the anterior or posterior sclera. Even though it has been known that the uveoscleral pathway accounts for some of the total outflow rate, the treatment over the uveoscleral pathway to increase outflow rate has been considered to be not as efficient as the one over the trabecular pathway for physiological and practical reasons.

1.2.5.4. The Treatment for the Management of IOP

The amount of the outflow the uveoscleral pathway account for is so different in each species that it accounts for 80 % in mice, 60% in monkies and 8% in rabbits [3]. Therefore, the expanded Goldmann equation is used to calculate the uveoscleral outflow rate [25].

$$F = F_s + F_i = (P_i - P_e) / R_s + F_i$$

F: the AH flow rate into and out of the anterior chamber

$\mathbf{F_s}$: the trabecular (pressure-sensitve) AH outflow rate

$\mathbf{F_i}$: the uveoscleral (pressure-independent) AH outflow rate

$\mathbf{P_i}$: IOP, $\mathbf{P_e}$: the pressure of episcleral vein (extraocular recipient)

$\mathbf{R_s}$: the resistance of trabecular AH outflow

It can be seen in the equation that the uveoscleral outflow rate is calculated using other measurements. However, the trabecular outflow is pressure-sensitive [26] and there is the possible introduction of errors in using the expanded Goldmann equations, indicating the basic information for the treatment can't be provided. It can be seen in Figure 1.5 that the uveoscleral outflow rate is not pressure-insensitive and the contribution to the management of IOP will be reduced at high IOP [3], leading to the reduced impact of the uveoscleral treatment on the reduction of IOP. As it can be seen in the Figure 1.3, AH exits the eye over the much larger scleral surface along the uveoscleral pathway, indicating that the treatment should be conducted over the larger surface. There is also not enough information on the outflow resistance distribution along the uveoscleral pathway. In the case of the trabecular pathway, the distribution of the resistance along the trabecular pathway has been known that JCT has the highest

resistance. Therefore, the optimal treatment can not be achieved over the uveoscleral pathway. In addition to this, there is the possible damage to the components such as choroid and ciliary body around the uveoscleral pathway.

Based on these reasons, it can be concluded that the treatment should be given over the trabecular pathway. Therefore, treatments will be introduced focused on this area.

1.3. Glaucoma and its Treatment

Glaucoma is a progressive optic nerve disease causing the selective loss of nerve fibers [27] leading to the visual field loss [27, 28] and its source and progress are different based on kind of glaucoma to be described later. Glaucoma is the second leading cause of blindness in the world [27] and 130,540 people lost sight from primary glaucoma in 2000 [29] and there are 300,000 new cases of glaucoma every year in US [30]. Looking at these studies, the effects of glaucoma associated visual loss on the economic and daily life such as treatment cost and accidents [31-38] can be estimated and the significance of effective glaucoma treatment can be recognized easily.

There are various kinds of glaucoma such as developmental glaucoma including congenital glaucoma caused by abnormal development like the root of the iris covering the surface of trabecular meshwork [9] and the secondary glaucoma caused by abnormal ocular and systemic conditions like new blood vessels covering the trabecular meshwork [39]. However, primary glaucoma, primary open angle glaucoma (POAG) and primary angle closure glaucoma (PACG), has been known to account for the majority of glaucoma occurring to people in the world. The review of the World Health Organization (WHO) showed that the cases of newly diagnosed POAG is estimated to be 2,400,000 per

year [40] and 3,000,000, out of 5,000,000 people who lost vision from glaucoma, became blind from POAG [41]. PACG is more frequent in Asia [42]. Therefore, in this section, the details of primary glaucoma will be introduced putting emphasis on POAG, more prevalent over the world.

1.3.1. Primary Open Angle Glaucoma (POAG)

1.3.1.1. Definition

The diagnostic criteria for POAG used in many studies are the optic nerve head and visual field damage [43, 44]. However, following the definition by the 1996 American Academy of Ophthalmology Preferred Practice Pattern, POAG is chronic, generally bilateral, often an asymmetrical disease with characterizing factors, glaucomatous optic nerve damage, adult onset, open, normal-appearing anterior chamber angles, and absence of known other causes of open angle glaucoma [45].

1.3.1.2. Risk Factors

It has been shown that the risk of POAG is increased over age [46] and the prevalence of POAG in specific races [46, 47], family with glaucoma history [47, 48] and elevated IOP [12]. However, IOP has been considered to be the most significant factor among others, because IOP is the uniquely treatable one. It has been believed in POAG that IOP is elevated by reduced AH outflow rate originating from the increased outflow resistance along the pathways [48] in possible association with decreased endothelial cell number [49] with thicker basement membrane [50, 51] and trabecular meshwork cells lost over age [52]. Various treatments that can be classified into medical, surgical, and laser treatment have been introduced to reduce IOP by reducing the production of AH or,

in most cases, the AH outflow rate resistance ultimately leading to the increased AH outflow rate.

1.3.1.3. Treatment of POAG

1.3.1.3.1. Medical (Drug) Treatment

Drugs have been used to lower IOP in various forms such as drop, aqueous solutions, ocular inserts and gels [52]. Considering AH dynamics that IOP is decided by the balance between the AH inflow and outflow of anterior chamber, theoretically, IOP can be reduced in two ways, increasing AH outflow and reducing AH production. For the case that the abnormally large amount of AH is secreted, medications can be selected to reduce the amount of AH secretion by interfering the AH production process described in the section of structure and physiology of the eye. For example, the enzyme carbonic anhydrate (CA), especially CA-II, was found to be present in nonpigmented epithelium of the ciliary processes supporting carbonic anhydrate's role in the transfer of sodium bicarbonate and fluid into AH [53]. Based on this discovery, carbonic anhydrate inhibitors (CAI) such as acetazolamide, methazolamide and ethoxzolamide have been used to reduce AH formation by interfering AH production process [53]. However, in most cases, medical treatment works the other way, because IOP is elevated in glaucomatous eyes by reducing the AH outflow and it should be more efficient to treat glaucoma by reducing the AH outflow resistance. For example, cholinergic agents such as pilocarpine and acecline widen the spaces in trabecular meshwork and the Schlemm's canal by stimulating the muscle of ciliary body to contract [9, 54], leading to the reduced AH resistance.

However, medical treatment has unavoidable disadvantages such as adhesion and tolerance from continuous usage over time, cost from effect reduced over time, and various side effects [9]. For example, CAIs have ocular side effects such as supraihroidal effusion, surface irritation, dryness, [9] systemic side effects such as anorexia, weight loss, and fatigue [9]. Cholinergic agents also have ocular side effects such as degraded vision by miosis, severe headache from muscle spasm, and accommodative myopia [9]. It is also hard to significantly reduce IOP and control the amount of reduced IOP with medical treatment.

1.3.1.3.2. Surgical Treatment

Surgical treatments for OPAG can be classified into three operations depending on the detailed approach [30]. Even though there is AH production reducing operation in surgical treatment, the majority of surgical treatment is AH outflow increasing operation.

Operations to improve extraordinary drainage of aqueous humor

It can be divided into the operation with a scleral flap such as trabeculectomy and without a scleral flap such as sclerectomy [30]. A trabeculectomy described in Figure 1.6 (a) is the operation to increase AH outflow by creating a partial-thickness flap of the sclera covering the opening between the anterior chamber and the subconjunctiva space to overcome the complications of full thickness operations [30]. The overall process is composed of dissecting a scleral flap, excising Schlemm's canal, and trabecular meshwork and suturing the flap [55]. Sclerectomy, described in Figure 1.6 (b), is to create the opening from anterior chamber to the conjunctival flap whole through the sclera [56]. Sclerectomy is used when visual loss is very severe and IOP should be reduced significantly to stop the progress of visual loss [56].

Operations to form paths for intraocular drainage of aqueous humor such as goniotomy

Goniotomy is to make the direct access to the Schlemm's canal by removing the tissues blocking the AH flow through the Schlemm's canal with a fine knife by incising the anterior chamber [30, 9].

Operations to reduce production of aqueous humor such as cyclodialysis

Cyclodialysis is to create the direct AH outflow communication between the anterior chamber and suprachoroidal space by separating ciliary body from a scleral spur [30]. The communication is created by inserting the tip of a spatula into the anterior chamber through the suprachoroidal and widening it by sweeping the spatula as shown in Figure 1.7 Cyclodialysis has disadvantages such as hemorrhage in the anterior chamber and stripping of the Descemete's membrane [30].

Surgical treatment is used especially when medical treatment does not work well, the amount of needed IOP reduction is too large, and the control over the amount of reduced IOP is needed. However, surgical treatment has disadvantages such as scar, bleeding, infection, and the structural damage to the eye from its unavoidable incisional procedures [12].

1.3.1.3.3. Laser Treatment

Laser Trabeculoplasty (LT) is more widely used POAG laser treatment. LT decreases outflow resistance by thermally burning the surface of trabecular meshwork as shown in Figure 1.8, causing the loss of endothelial cells, disruption, scaring, and shrinkage of the trabecular beam leading to the adjacent opening of pore by tension [9]. LT also causes the AH outflow resistance reducing biochemical response of treated

trebecular meshwork tissues [12]. The most widely used types of LT are argon laser trabeculoplasty (ALT) and selective laser trabeculoplasty (SLT) with Q switched frequency-doubled Nd:YAG laser.

ALT is advantageous in that it has much reduced compliance, side effect issue, and it is effective as initial therapy to reduce IOP such that 63% of patients maintained IOP control 1 year after ALT [57, 58]. However, the continuous use of ALT is limited by mass destruction of the cell and the trabecular beams around the treated area [9]. ALT also has disadvantages such as unsatisfactory long-term effect and the possible failure because trabecular meshwork (TM) is partially burned [9].

SLT works using the same mechanism as introduced in the ALT mechanism. The use of SLT is advantageous over ALT since SLT has a greater IOP reducing effect than the ALT retreatment in patients with ALT failure [9]. SLT is also advantageous since it reduces tissue destruction when compared to ALT. This can be explained with more confined heat deposition to the tissue due to the much shorter pulse used in SLT [9], proposing the potential of more advantageous laser treatments by the continuous reduction of pulse duration into shorter regime.

1.3.2. Primary Angle Closure Glaucoma (PACG)

1.3.2.1. Definition

PACG is defined as “appositional or synechial closure of the anterior chamber angle closed by relative pupillary block in the absence of other causes of angle closure” [45]. The most common way that PACG occurs is when AH flow to the anterior chamber from the posterior chamber is blocked by the apposition of the iris pupil against the lens, leading to a pressure increase in the posterior chamber [9]. Then, the peripheral iris will

be pushed upward, called iris bombe described in Figure 1.9 (a), and the AH flow into trabecular meshwork is reduced. If the peripheral iris keeps pushed, AH outflow into trabecular meshwork (TM) can be blocked by the iris as shown in Figure 1.9 (b). The increased IOP is dependent on the area of TM covered by the iris. IOP can be increased from 20 to 40 IOP when the entire TM is covered [9].

1.3.2.2. Risk Factors

Shallow anterior chamber, short axial length, and small corneal diameters are well known risk factors, but the shallow anterior chamber is the most consistent factor [60]. A shallow anterior chamber is inherited, related to age, gender, and race [55, 60]. The prevalence of PACG is 4 – 5 times higher in women [60] and 3.5 – 6 times in Inuit with the first degree relatives of affected parents and in family members of affected Chinese parents [61].

1.3.2.3. Treatment of PACG

1.3.2.3.1. Medical (Drug) Treatment

Additionally to lowering IOP, medical treatment for PACG includes clearing the cornea to make a laser treatment and laser iridotomy available [9]. Medical treatment is composed of beta-adrenergic blocking agents and topical carbonic anhydrase inhibitors (CAI) [9]. For example, 1 or 2% of the pilocarpine, can be used to open the angle and stretch the iris to make the iridotomy available [9].

1.3.2.3.2. Surgical Treatment

Iridectomy is the act of excising a piece of the iris to deepen the anterior chamber and is the most frequently used surgical treatment for pupillary block, especially when laser iridectomy is not available due to poorly visible iris from the opaque cornea or

occlusion from intraocular inflammation [56]. The key process is to create the opening through the limbus, undermining conjunctiva [56].

1.3.2.3.3. Laser Treatment

Laser iridotomy is the process that creates a thick hole in the iris as shown in Figure 1.10. A hole can be created with surgical procedure, called iridectomy before the laser was introduced. However, an iridectomy has many complications such as infection and would leak from the incisional penetration of surgical tools [9]. The argon laser was introduced first to create a whole, but the Nd:YAG laser is preferred because of its advantage of property without the disadvantages of the argon laser such as coagulative effect in the adjacent stroma [9].

A Gonioplasty (GPL) is performed to widen the angle with contraction of the iris by heating the iris tissue neighboring the root of the iris [30]. When the heat is applied to the iris tissue by a laser, the tissues around the heated spot are contracted. If the tissues near the root of the iris are heated, the tissues at the iris root move deeper from the contractions [30]. If the tissues near the end of iris are heated, the pupillary block can be opened by the contraction [62, 63]. This treatment can be used as a supporting treatment for other ones such as laser a trabeculoplasty and a laser iridotomy [30]. However, GPL has disadvantages such as the potential of immediate postoperative IOP spike, distortion of the pupil, and possible heat of the endothelium in the eye of the shallow anterior chamber [30]. It is difficult to control the amount of IOP reduction also.

Taking a look at the glaucoma treatments that have been developed, it can be seen that the history of developing treatments is the process to achieve the treatment with advantages of medical and surgical treatments, nonincisional and controllable one. As

lasers showed the potential of this treatment, various lasers with the better properties of the interaction with tissues have been introduced in different methods over the development of lasers. As the new laser with reduced pulse duration was recently introduced with the advantageous property, the attention has been drawn to the development of methods that can make advantage of this laser for the eye treatment. In the next chapter, the details of that laser, called a femtosecond laser, will be introduced.

1.4. Laser Tissue Interaction

Since the potential of the laser microsurgery was proposed by the dissection of chromosome with an argon laser [64, 65], the development of laser treatment has been led by the advance of laser technology. The range of available laser parameters in laser tissue experiments was expanded by laser technology development, thus the mechanism of laser energy deposition into the tissue, and the effect of each laser on it could be investigated [66 - 68] with a wide range of pulse durations. It was found that the pulsed laser has more advantageous interaction property with tissue than the continuous wave laser and the major improvement on the laser tissue interaction could be made by reducing the pulse duration that can make more precise treatment available [69]

The eye treatment has been the major application field of the microsurgery by a laser, because the extreme precision is needed that can never be achieved by traditional surgical techniques. Additionally, traditional surgical treatment has the limitation of using unavoidable incisional procedures performed with surgical blades that can cause bleeding, scar [30]. Argon laser has been widely used, but lasers with more advantageous

interaction with tissues, such as Nd:YAG laser [70], were introduced to perform more advanced treatments.

In this section, the fundamentals of the laser tissue interaction will be discussed, Initially laser-tissue interaction mechanisms of argon laser and Nd:YAG laser will be compared. Then, the femtosecond laser, which came into the spotlight with the potential of alternative laser for more advantageous treatments, will be introduced.

1.4.1. Deposition of Laser Energy into the Tissue

1.4.1.1. Linear Absorption

In the case of linear absorption the photon energy of the laser is in resonance with the electron excitation energy of the molecules in the tissue. Thus, if the laser beam irradiates the tissue, the absorption of the photon promotes the level of electrons to the excitation level [72]. Then, collisions of electrons and nonradiative relaxation convert this energy into the heat, leading to temperature increase in the tissue [70]. In the wavelength of ultraviolet (UV) and near infrared (NI) region ($\lambda \approx 780 - 2500$ nm), melanin and hemoglobin are strong and dominant absorbing molecules in ocular tissues and thermal effect are dependent on the responses of these molecules to a laser beam [72, 73].

The extent of thermal tissue damage is dependent on the temperature increase. No irreversible damage occurs up to 45 ^{o}C, tissue temperature, and denaturation of biomolecules, coagualation effect, occurs from 60 ^{o}C [70]. The extent of effect is proportional to irradiation time and power of laser beam in photocoagulation, the working mechanism in ALT and SLT. The laser parameters are $\lambda = 488$ to 514 nm, 0.1 s irradiation time for ALT and $\lambda = 532$ nm, 3 ns pulse duration for SLT [71]. Comparing

the irradiation time of each one to 1μs [74], the thermal relaxation time of melanin, it can be seen that SLT with shorter duration than the thermal relaxation time, should have much reduced effect on the tissues adjacent to the treated spot.

1.4.1.2. Nonlinear Absorption

1.4.1.2.1. Definition and Free Electron Generation

In the case of nonlinear absorption the energy of the laser photons are smaller than the differences of the electron energy levels. Thus, the absorption of multiple electrons occurs simultaneously to achieve excited state. This requires high electron density therefore nonlinear absorption usually occurs when the irradiance of the laser beam is higher than $10^{10} \sim 10^{13}$ W/cm^2 [72]. If electrons absorb energy higher than the ionization potential, the medium is ionized and free electrons are generated. Free electrons can be generated by the one of the following ionization mechanisms in tissue as described in Figure 1.11 [72, 75].

Multiphoton Ionization

In the case of Multiphoton ionization free electrons are created with the absorption of several photons simultaneously [72]. Therefore, it does not take much time and space to generate free electrons via multiphoton ionization and seed electron, existing free electron, is not needed.

Avalnche Ionization

At least one free electron, a seed electron, is needed for avalanche ionization. Free electrons absorb the laser beam energy and this energy is converted into the kinetic energy. If the kinetic energy of electron is increased high enough, free electrons can be generated by the collision between free electrons and molecules.

1.4.1.2.2. Laser Induced Optical Breakdown (LIOB)

Increased intensity and radiant time lead to the increase of free electrons density by the combination of ionization processes mentioned in the previous section. If the density of free electrons reaches $10^{21}/cm^3$ plasma is formed and this process is called optical breakdown [72]. This laser induced optical breakdown (LIOB) initiates photodisruption, the phenomenon that the tissue is disrupted by the high-power ionizing laser pulses [76].

Once plasma is formed, the kinetic energy of free electrons is converted into the temperature and pressure increase by the collisions with other molecules. As described in Figure 1.12 [66], the plasma is expanded by increased pressure and temperature, leading to the tension stress on the material by the expanding the plasma [77]. The shock wave is emitted when the velocity of the plasma expansion is reduced to the subsonic from the initial hypersonic velocity [78]. When the liquid is ruptured by the tensile stress under the isothermal condition, it is called 'cavitation' [69]. Bubbles are created and imploded when the plasma is continuously expanded [76, 79] and these bubbles are called 'cavitation bubbles' and used as criteria of the occurrence of photodisruption [69]. Shock wave and cavitation bubbles contribute to the disruption effect of a laser, but, as described in Figure 1.12 [66], their effects are on the space plasma expansion, reducing the precision of laser treatment [80]. Therefore, it can be concluded that the evaporation of plasma is the main effect for photodisruption and shock wave and cavitation bubble are considered to be the unwanted side effects [80].

1.4.1.2.3. The Effect of Pulse Duration on Photodisruption

The wider range of laser parameters could become available over the development of laser technology. It was found that the pulse duration is the laser parameter with the effects on the property of the deposition of laser beam energy into the tissue [80]. The effect of the pulse duration on the laser tissue interaction can be explained along the photodisruption process.

Ionization Processes

As the pulse duration is reduced, the contribution of avalanche ionization to LIOB is reduced due to the lack of time to absorb and converse the beam energy into the kinetic energy of electrons, followed by collisions with other electrons, molecules [75]. Therefore, the contribution by the multiphoton ionization is increased to LIOB over the reduced pulse duration, leading to the change in other properties of laser tissue interaction to be explained later.

More Consistent Electron Density in Plasma

An existence of seed electron, basic necessity of avalanche ionization, is dependent on the molecular structure, especially impurities, of the irradiated material [70] and the collisions between molecules and electrons cannot be controlled. On the contrary, multiphoton ionization is not affected by seed electrons. Therefore, the density of free electrons in plasma can be maintained more consistently by reducing the pulse duration.

Reduced LIOB Threshold

Irradiance threshold (W/cm^2) for LIOB is increased as the pulsed duration is reduced, because, as explained in 'ionization process' section, the contribution by avalanche ionization to the plasma formation is reduced. However, as shown in Figure 1.13 [81], the

energy threshold is reduced over the shorter pulse duration, because there is no time for the recombination of free electrons during the short pulse duration [69].

Reduced Side Effects

Figure 1.14 [81] shows the shock wave pressure over the radius in water generated by lasers with different duration, 150 fs and 60 ps [81]. It can be seen that shock wave pressure is reduced rapidly when it is generated by 150 fs laser, meaning the rapid reduction of the shock wave propagation velocity. Therefore, it can be concluded that the space under the effect of shock wave is reduced with shorter pulse duration of a laser.

Cavitation bubble is generated, expanded while the plasma is expanded. As the pulse duration is reduced, the plasma expansion time is also reduced. Therefore, cavitation bubble is expanded for the shorter period, leading to the reduced diameter of cavitation bubble [81]. It was shown that when measured 1 ms after the irradiation of a laser in corneal tissue, the diameter of cavitation bubble is 14 μm by femtosecond pulses and 80 μm by picosecond pulses [79].

Confined Treatment

If the pulse duration is reduced into the femtosecond regime, temperature is elevated within a few to tens of picosecond much shorter than 1 μs, the heat relaxation time for melanin [30, 72], indicating the thermoelastic stress is confined in the focal volume [30]. Adding this effect to the reduced side effect, the confined effect of the short duration pulse can be easily expected [69], indicating the potential of more precise surgery of femtosecond pulse lasers.

1.4.2. Optical Penetration Depending on the Wavelength of the Pulse

As it was mentioned, lasers were introduced to the eye treatment to develop the noninvasive treatments. To make advantage of this beauty of laser treatments, subsurface laser treatment should be available without any damage to the surface of tissue and laser beam should penetrate and be focused into the tissue deep enough to treat the target area below the surface. When laser beam is irradiated to the tissue, the following five phenomena can occur [9];

1) Reflection: when laser beam is reflected backward at the surface of tissue in the small portion.
2) Refraction: when laser beam passes, being refracted, through the surface, it is affected by the incidence angle and the refractive index difference between two media of air (1.0) and sclera (1.37).
3) Absorption: when energy of beam is absorbed by the molecules depending on the absorbing coefficient in the function of wavelength, indicating the absorption can be minimized by selecting the proper wavelength.
4) Scattering: bend of light wave propagation when the traversing wave is faced to the local change of the media.
5) Traverse through tissue: the photons passing through the tissue in the propagating direction of the beam.

Small portion of a beam is reflected and refraction can be reduced by introducing the glass and adjusting the penetration angle of beam into the tissue. Therefore, it can be concluded that photons are affected in the irradiance by absorption and in focus beyond the tissue by scattering. Refractive index and the micro structure inside the material have the effect on scattering and it is difficult to predict the scattering by the calculation.

However, it has been known that scattering is decreased over wide range of wavelength, as the wavelength is increased [70] and the absorption of photons is affected by wavelength [73] and near infrared laser beam with wavelength from 780 nm to 2.5 μm [70] can penetrate deep into the biological tissues due to its low absorption and scattering coefficients inside the biological tissues [82]. Therefore, it should be the best approach to select the wavelength of laser beam experimentally by investigating the penetration depth and focus into or beyond the target tissue over the near infrared wavelength.

1.4.3. Selecting the Optimal Laser Parameters for the Treatment of the Eye

The optimal wavelength should be selected for each laser treatment, because the absorption and scattering property of each tissue is different depending on wavelength. The scattering through sclera was investigated by monitoring the focus over near infrared wavelength [83]. Figure 1.15 shows that the wavelength to minimize the scattering is 1700 nm [83].

The absorption of a laser beam was investigated over wavelength as shown in Figure 1.16 [85]. It can be seen that there are three peak points of transmission and the one of them is 1700 nm, indicating the absorption is minimum at those wavelengths. Combining the results shown in Figure 1.15 and Figure 1.16, it can be concluded that 1.7 μm is the optimal wavelength of a laser beam for the eye treatment that minimize the scattering and absorption.

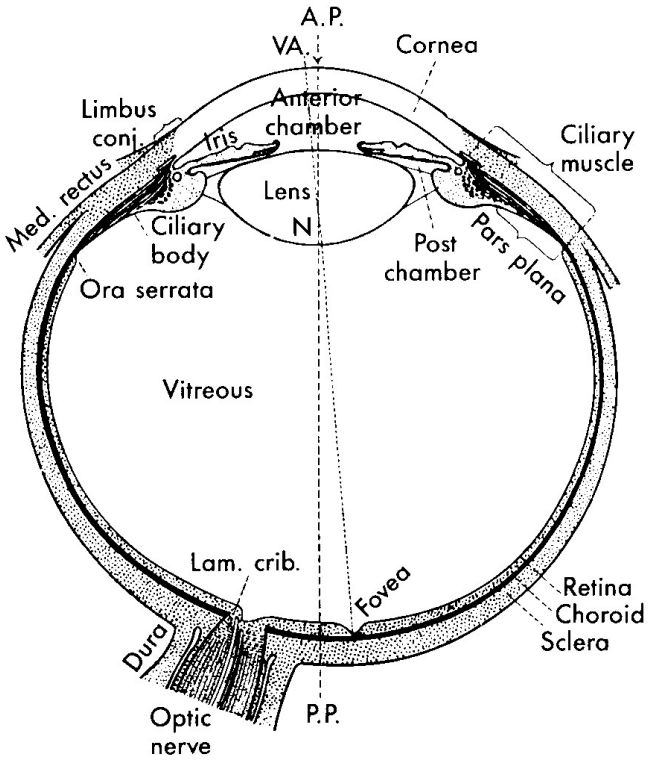

Figure 1.1. Overall structure of the eye (P.P: Posterior Pole, A.P: Anterior Pole, VA: Visual Axis) [2]. Light forms image on retina through cornea and lens. Each structure adjusts the structure to make a sharp image on fovea.

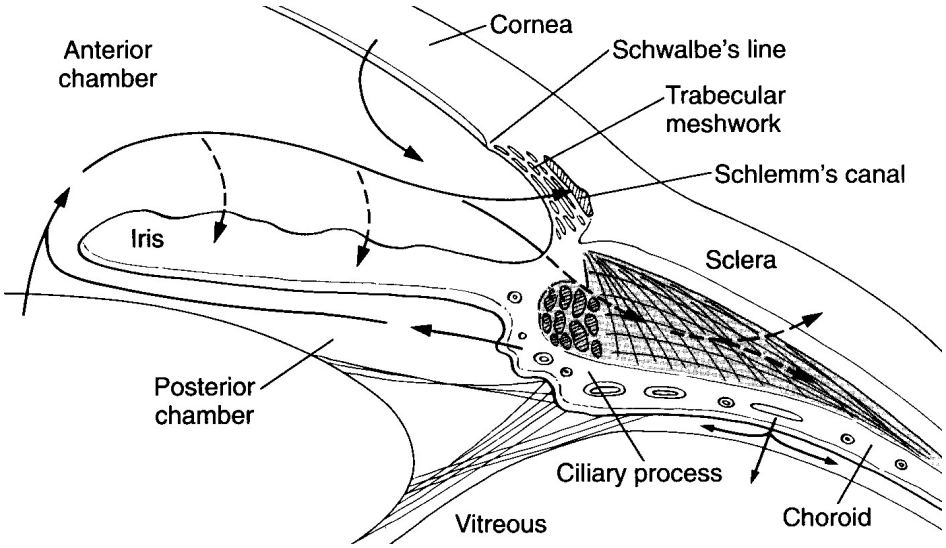

Figure 1.2. The structure of the parts involved in AH flow [26]. AH is secreted from ciliary process and exits the eye through pathways.

Components	Ciliary Processes (mmol/kg H_2O)	Anterior/Posterior Chamber (mmol/kg H_2O)
Na	146	164
Cl	109	134
HCO_3	28	20
Ascorbate	0.04	1.06
Glucose	6	3

Table 1.1. Composition of AH depending on position [10].

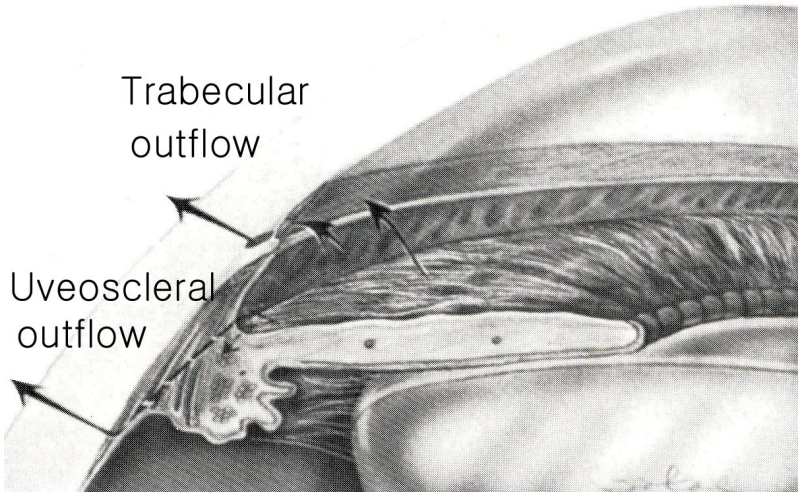

Figure 1.3. AH outflows through trabecular and uveoscleral pathway [3].

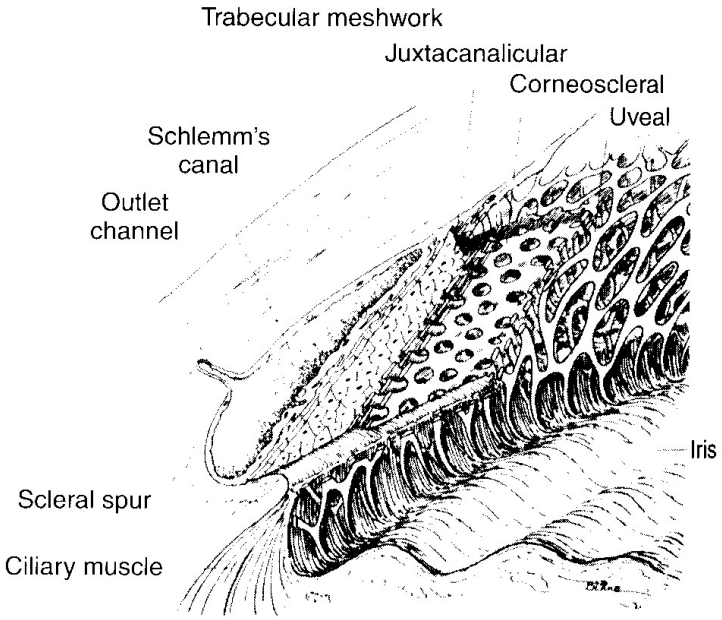

Figure 1.4. Components of trabecular meshwork [6]. AH flows through uveal, corneoscleral meshwork and juxtacanalicular meshwork into Schlemm's canal.

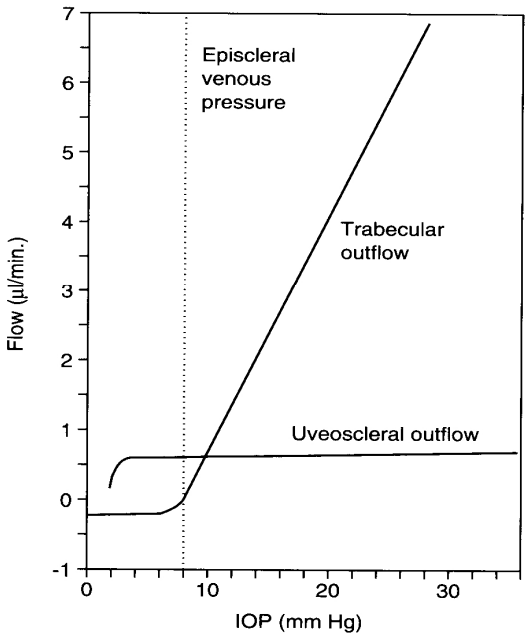

Figure 1.5. Change of the amount of AH outflow through each pathway over the IOP increase [26].

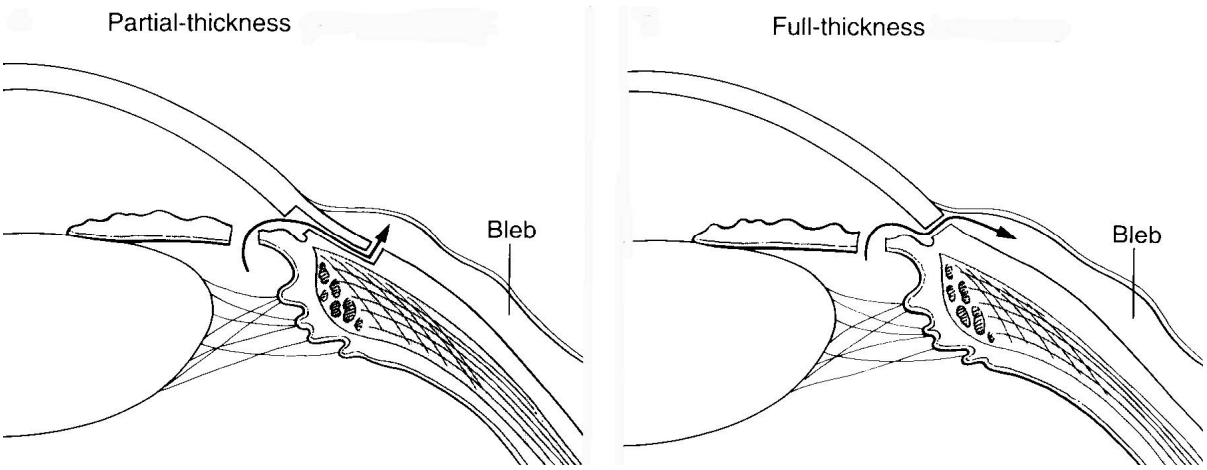

Figure 1.6. Extraordinary drainage creating operations ((a) Trabeculectomy, (b) Sclerectomy) [26].

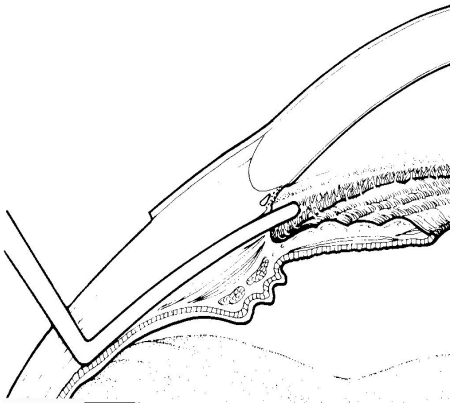

(a)

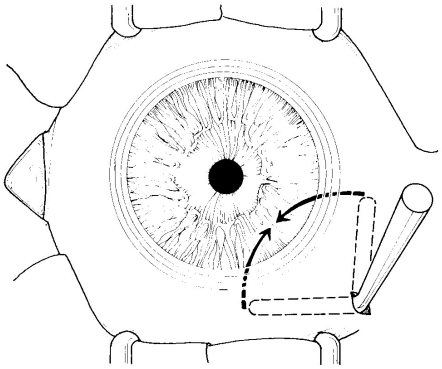

(b)

Figure 1.7. Operation of cyclodialysis ((a) Insertion of a spatula, (b) Widening the communication) [30].

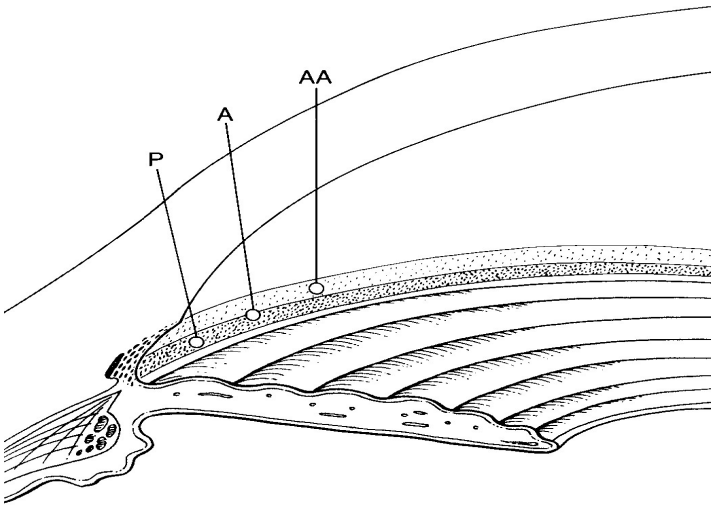

Figure 1.8. Location of laser burns in ALT and SLT (A: junction of pigmented and nonpigmented TM, AA: completely in the nonpigmented meshwork, P: completely in the pigmented meshwork) [26].

(a)

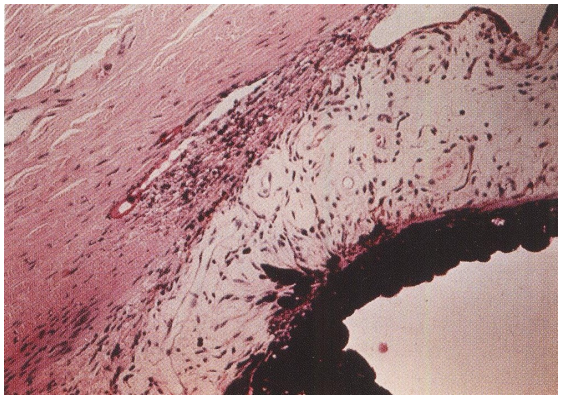

(b)

Figure 1.9. PACG cased by iris bombe and blocked TM ((a) PACG by iris bombe, (b) Light micrograph of blocked TM) [9].

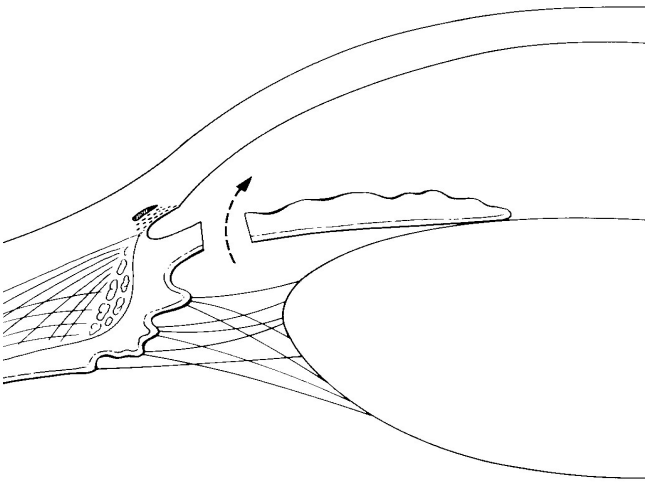

Figure 1.10. Hole in iris by laser iridotomy for AH flow through the hole [26].

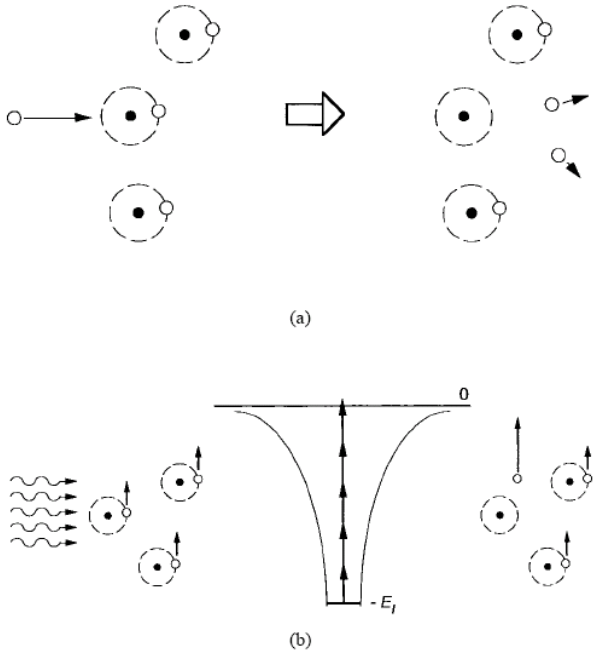

Figure 1.11. Schematic of (a) Avalanche ionization by the collision and (b) Multiphoton ionization by simultaneous absorption of several photons [75].

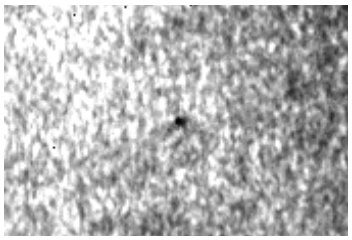

(a) 25 ps

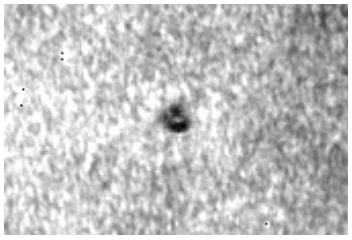

(b) 400 ps

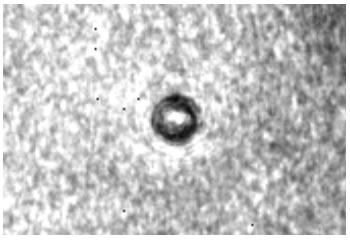

(c) 1.6 ns

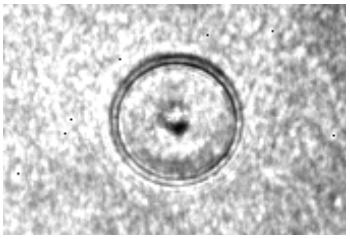

(d) 6.4 ns

Figure 1.12. The description of shock wave and cavitation bubble generation process over time delays ((a) Plasma formation, (b), (c) Plasma expansion and (d) Emission of shock wave) [66].

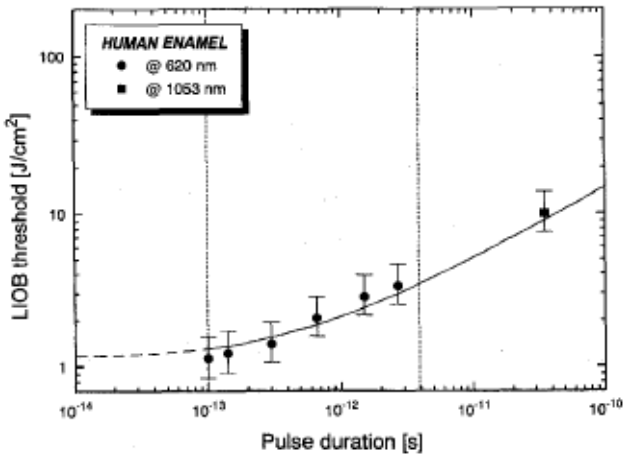

(a)

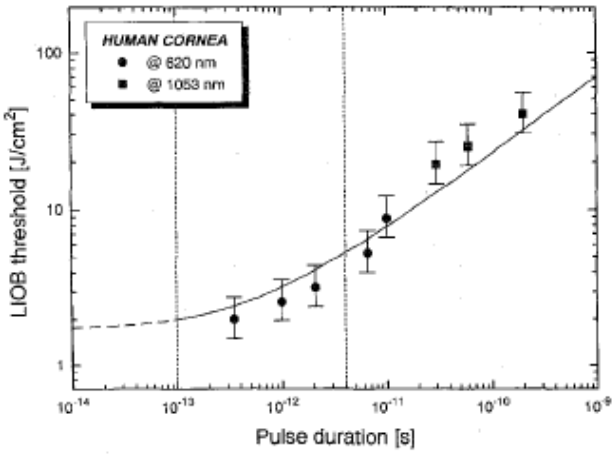

(b)

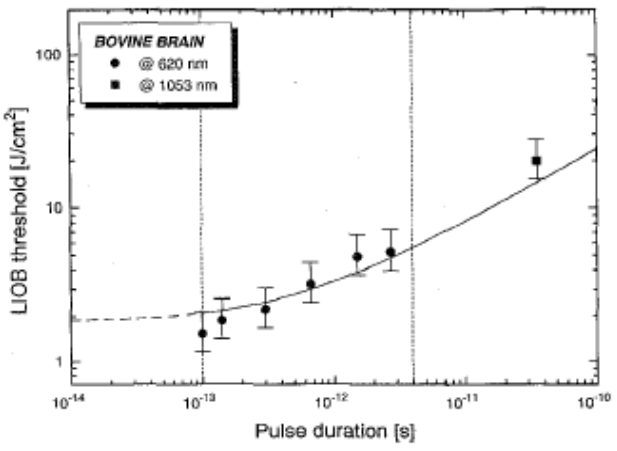

(c)

Figure 1.13. LIOB threshold over pulse duration on the surface of various materials ((a) Human enamel, (b) Human corneal tissue, (c) Bovine brain tissue**)** [81].

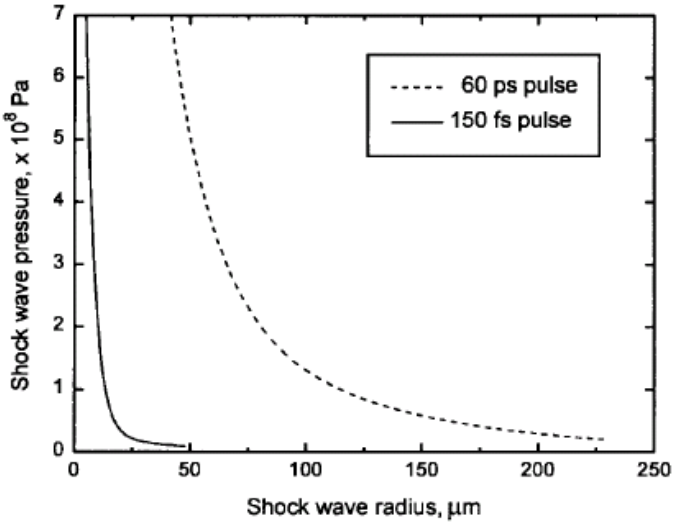

Figure 1.14. Shock-wave pressure as a function of the shock-wave radius in water generated by 150 fs and 60 ps laser pulses [81].

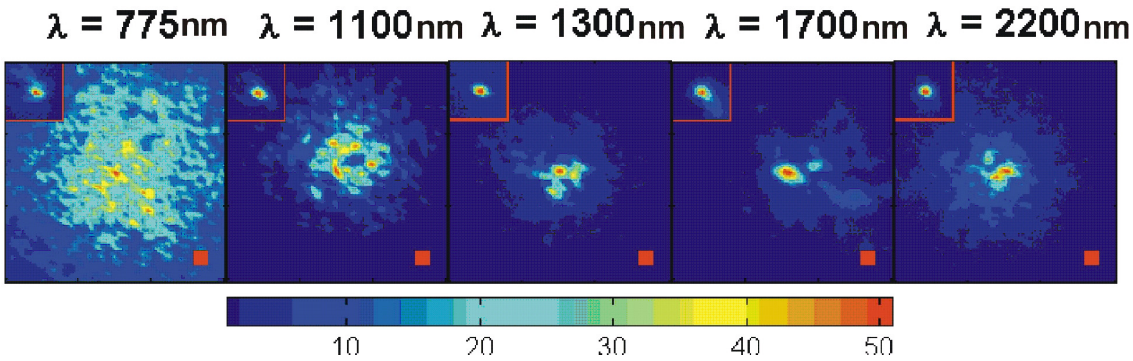

Figure 1.15. Focus beyond the sclera over wavelength [83]. Each side of red square at right bottom is 5 μm. The spot in the upper left is the minimum spot without tissue.

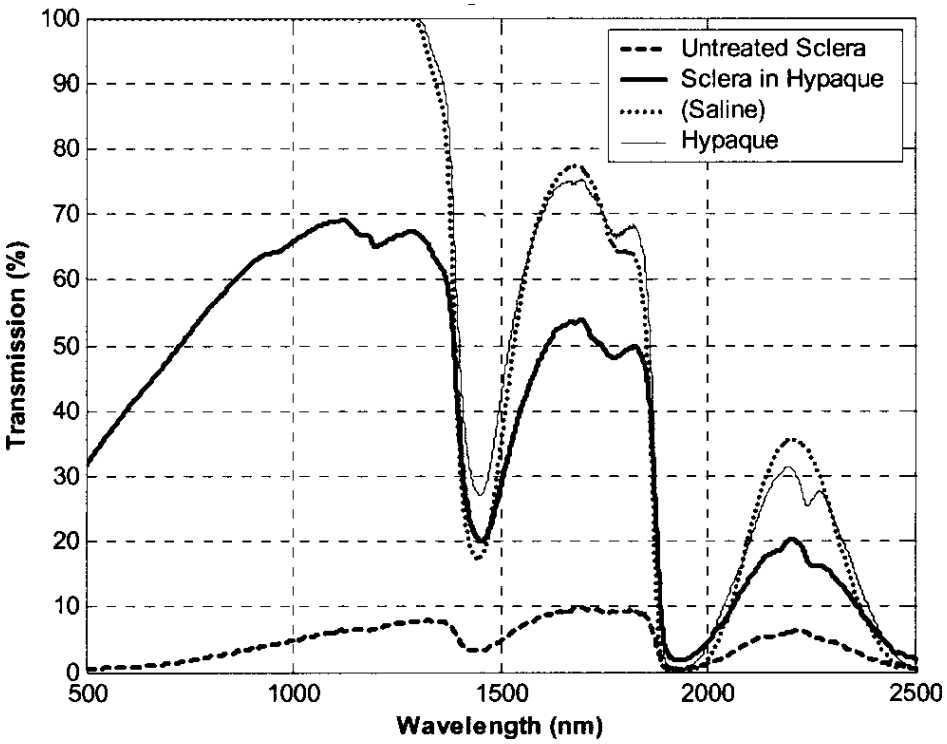

Figure 1.16. Transmission over wavelength [84]. Magnitude of transmission is different in each treatment of sclera before the measurement, but the scattering is dependent on wavelength regardless of the type of treatment.

1.5. References

[1] R. E. Records, *Physiology of the human eye and visual system*. Hagerstown, MD: Harper & Row, 1979.

[2] M. P. Fautsch and Johnson DH, "Aqueous humor outflow: What do we know? Where will it lead us?" *Investigative Ophthalmology & Visual Science*, vol. 47, pp. 4141-4187, 2006.

[3] P. L. Kaufman and A. Alm, *Adler's physiology of the eye.9th edition*. St. Louis: Mosby Year Book, 1992.

[4] V. B. Mountcastle, *Medical Physiology*. St. Louis: Mosby Year Book, 1980.

[5] C. W. Oyster, *The human eye. Structure and Function*. Southerland, MA: Sinauer Associates, 1999.

[6] P. L. Kaufman and A. Alm*, Adler's physiology of the eye: clinical application. 10th edition.* St. Louis: Mosby Year Book, 2003.

[7] P. G. Watson and R. D. Young, "Scleral structure, organization and disease. A review," *Experimental Eye Research*, vol. 78, pp. 609-623, 2004.

[8] M. M. Civan and A. D. C. Macknight, "The ins and outs of aqueous humour secretion," *Experimental eye research*, vol. 78, pp. 625-631, 2004.

[9] J. C. Morrison and I. P. Pollack, *Glaucoma: Science and Practice*. New York: Thieme Medical Publishers, 2003.

[10] A. D. C. Macknight, C. W. MacLaughlin, D. Peal, R. D. Purves, D. A. Carre, and M. M. Civan, "Formation of the aqueous humor," *Clinical & Experimental Pharmacology and Physiology*, vol. 27, pp. 100-106, 2000.

[11] M. M. Civan, "Transport by the ciliary epithelium of the eye," *News in Physiological Science,* vol. 12, pp. 158-162, 1997.

[12] T. L. Maus, W. F. Young, and R. F. Brubaker, "Aqueous flow in humans after adrenalectomy," *Investigative Ophthalmology & Visual Science,* vol. 35, pp. 3325-3331, 1994.

[13] N. A. Farahbakhsh, "Purinergic signaling in the rabbit cililary body epithelium," *Journal of Experimental Zoology*, vol. 300, pp. 14-24, 2003.

[14] H. Davson and L. T. Graham, *The Eye (Comparative Physiology)*. New York: Academic Press, 1974.

[15] W. M. Grant, "Experimental aqueous perfusion in enucleated human eyes," *Archive of Ophthalmology*, vol. 69, pp 783-801, 1963.

[16] M. Johnson, "What controls aqueous humor outflow resistance?" *Experimental Eye Research,* vol. 82, pp. 545-557*,* 2006.

[17] R. D. Ten Hulzen and D. H. Johnson, "Effect of fixation pressure on juxtacanalicular tissue and Schlemm's canal," *Investigative Ophthalmology & Visual Science*, vol. 37, pp. 114-124, 1996.

[18] R. A. Moses, "Circumferential flow in Schlemm's canal," *American Journal of Ophthalmology*, vol. 88, pp. 585-591, 1979.

[19] E. M. Van Buskirk, "Changes in the facility of aqueous outflow induced by lens depression and intraocular pressure in excised human eyes," *American Journal of Ophthalmology*, vol. 82, pp. 736-740, 1976.

[20] R. A. Moses, "The effect of intraocular pressure on resistance to outflow," *Survey of Ophthalmology*, vol. 22, pp. 88-100, 1977.

[21] Y. E. Batmanov, "Structure of the eye drainage system in man," *Vestnik. Oftal'mologi*, vol. 4, pp 27-31, 1968.

[22] R. Rosenquist, D. Epstein, S. Melamed, M. Johnson, and W. M. Grant, "Outflow resistance of enucleated human eyes at two different perfusion pressures and different extents of trabeculectomy," *Current Eye Research*, vol. 8, pp. 1233-1240, 1989.

[23] J. B. Wise and S. L. Witter, "Argon laser therapy for open-angle glaucoma. A pilot study," *Archive of Ophthalmology*, vol. 97, pp. 319-322, 1979.

[24] E. M. Van Buskirk, V. Pond, R. C. Rosenquist, and T. S. Acott, "Argon laser trabeculoplasty. Studies of mechanism of action," *Ophthalmology*, vol. 91, pp. 1005-1010, 1984.

[25] R. F. Brubaker, "Mechanism of action of biomatoprost (LumiganTM)," *Survey of Ophthalmology*, vol. 45, S. 347-351, 2001.

[26] S. M. Podos and M. Yanoff, *Textbook of ophthalmology*. Philadelphia, PA: Gower Medical Pub, 1994.

[27] H. Quigley, E. Addicks, W. Green, and A. Maumenee, "Optic nerve damage in human glaucoma, II: the site of injury and susceptibility to damage," *Archive of Ophthalmology*, vol. 99, pp. 635-649, 1981.

[28] J. S. Distelhorst and G. M. Hughes, "Open-Angle Glaucoma," *American Family Physician*, vol. 67, pp.1937-1944, 2003.

[29] H. A. Quigley, "Number of people with glaucoma worldwide," *British Journal of Ophthalmology*, vol. 80, pp. 389-393, 1996.

[30] J. V. Thomas, C. V. Belcher III, and R. J. Simmons, "Glaucoma Surgery," St. Louis: Mosby Year Book, 1992.

[31] H. A. Quigley and S. Vitae, "Model of open-angle glaucoma prevalence and incidence in the United States," *Investigative Ophthalmology & Visual Science*, vol. 38, pp. 83-91, 1997.

[32] R. J. Glynn, J. M. Seddon, J. H. Krug, C. R. Sahagian, M. R. Chiavelli, and E. W. Campion, "Falls in elderly patients with glaucoma," *Archive of Ophthalmology*, vol. 109, pp. 205-210, 1991.

[33] C. Owsley, G McGwin, and K. Ball, "Vision impairment, eye disease, and injurious motor vehicle crashes in the elderly," *Ophthalmic Epidemiology*, vol. 5, pp. 101-113, 1998.

[34] M. R. Wilson, A. L. Coleman, E. G. Bing, I. F. Sasaki, K. Berlin, J. Winters, and A. Lai, "Functional status and well-being in patients with glaucoma as measured by the Medical Outcomes Study Short Form-36," *Questionnaire of Ophthalmology*. vol. 105, pp. 2112-2116, 1998.

[35] M. B. Sherwood, A. Garcia-Siekvizza, M. I. Meltzer, A Herbert, A. F. Burns, and S. McGorray, "Glaucoma's impact on quality of life and its relation to clinical indicators: a pilot study," *Ophthalmology*, vol. 105, pp. 561-566, 1998.

[36] P. Gutierrez, M. R. Wilson, C. Johnson, M Gordon, G. A. Cioffi, R. Ritch, M. Sherwood, K. Meng, and C. M. Mangione, "Influence of glaucomatous visual field loss on health-related quality of life," *Archive of Ophthalmology*, vol. 115, pp. 777-784, 1997.

[37] P. K. Parrish II, J. J. Gedde, I. U. Scott, W. J. Feuer, J. C. Schiffman, C. M. Mangione, and A. MontenegroPiniella, "Visual function and quality of life among patients with glaucoma," *Archive of Ophthalmology*, vol. 115, pp.1447-1455, 1997.

[38] G. Kobelt, U. G. Gerdtham, and A. Alm, "Cost of treating primary open-angle glaucoma and ocular hypertension," *Journal of Glaucoma*, vol. 7, pp. 95-104, 1998.

[39] S. Gartner and P. Henkind, "Neovascularization of the iris (rubeosis)," *Survey of Ophthalmol*, vol. 22, pp. 291, 1978.

[40] N. Ashton, "The exit pathway of the aqueous," *Transaction of Ophthalmology Society of UK*, vol. 80, pp. 397, 1960.

[41] H. A. Quigley, "Number of people with glaucoma worldwide," *British Journal of Ophthalmology*, vol. 80, pp. 389-393, 1996.

[42] J. L. Rivera, N. P. Bell, and R. M. Felman, "Risk factors for primary open angle glaucoma progression: what we know and what we need to know," *Current opinion in Ophthalmology*, vol. 19, pp. 102-106, 2008.

[43] R. Thomas, G. C. Sekhar, and R. Parikh, "Primary angle closure glaucoma: a developing world perspective," *Clinical and experimental Ophthalmology*, vol. 35, pp. 374- 378, 2007.

[44] F. C. Hollows and P. A. Graham, "Intraocular pressure, glaucoma, and glaucoma suspects in a defined population," *British Journal of Ophthalmology*, vol. 50, pp. 570-586, 1966.

[45] M. C. Leske, A. M. S. Connell, A. P. Schachat, and L. Hyman, "The Barbados Eye Study: prevalence of open-angle glaucoma," *Archive of Ophthalmology*, vol. 112, pp. 821-829, 1994.

[46] American Acamemy of Ophthalmology. Glaucoma Panel, *Preferred Practice Pattern of Primary Open-Angle Glaucoma*. San Francisco, Callf: American Academy of Ophthalmology; 1996.

[47] B. Nemesure, M. C. Leske, Q. He, and N. Mendell, "Analyses of reported family history of glaucoma: a preliminary investigation: The Barbados Eye Study Group," *Ophthalmic Epidemiology*, vol. 3, pp.135-141, 1996.

[48] J. M. Tielsch, A. Sommer, J. Katz, H. A. Quigley, J. D. Gottsch, J. C. Javitt, J. F. Martone, R. M. Royall, K. A. Witt, and S. Ezrine, "Racial variation in the prevalence of primary open-angle glaucoma - The Baltimore Eye Survey*," Journal of the American Medical Association*, vol. 266, pp. 369-374, 1991.

[49] Z. Hu, Z. L. Zhao, and F. T. Dong, "An epidemiologic investigation of glaucoma in Beijing and Shun-yi County," *Chinese Journal of Ophthalmology*, vol. 25, pp. 115-118, 1989.

[50] J. Alvarado, C. Murphy, and R. Juster, "Trabecular meshwork cellularity in primary open-angle glaucoma and nonglaucomatous normals," *Ophthalmology*, vol. 91, pp. 564, 1984.

[51] J. S. Speakman and T. S. Leeson, "Site of obstruction to aqueous outflow in chronic simple glaucoma," *British Journal of Ophthalmology*, vol. 47, pp. 21, 1962.

[52] N. Congdon, F. Wang, and J. M. Tielsch, "Issues in the epidemiology and population-based screening of primary angle-closure glaucoma," *Survey of Ophthalmology*, vol.36, pp. 411-243, 1992.

[53] P. J. Wistrand, M. Schenholm, and G. Lonnerholm, "Carbonic-anhydrase isoenzymes CA-I and CA-II in the human eye," *Investigative Ophthalmology & Visual Science*, vol. 27, pp. 419-428, 986.

[54] J. M. H. Preuss and R. G. Gordie, "Muscarinic cholinoceptor subtypes mediating tracheal smooth muscle contraction and inositol phosphate generation in guinea pig and rat," *European Journal of Pharmacology*, vol. 372, pp. 269-277, 1999.

[55] P. H. Alsbirk, "Primary angle-closure glaucoma. Oculometry, epidemiology, and genetics in a high risk population," *Acta Ophthalmoogica,* vol. 127, pp. 5-31, 1976.

[56] R. Ritch, M. R. Shields and T. Krupin, "The glaucomas: Gluacoma Therapy. 2nd Ed," Missouri: Mosby-Year, 1996.

[57] J. Krug, M. Chiavelli, and G. Borawski,et al, "The Glaucoma Laser Trial (GLT) and Glaucoma Laser Trial follow-up- study .7. Results," *American Journal of Ophthalmology*, vol. 120, pp. 718-731, 1995.

[58] J. V. Thomas, A. EL-Mofty, E. E. Hamdy, and R. J. Simmons, "Argon Laser trabeculoplasty as initial therapy for glaucoma," *Archive of Ophthalmology*, vol. 102, pp.702-703, 1984.

[59] K. F. Damji, K. C. Shah, W. J. Rock, H. S. Bains, and W. G. Hodge, "Selective laser trabeculoplasty v argon laser trabeculoplasty: a prospective randomized clinical trial," *British Journal of Ophthalmology*, vol. 83, pp. 718-722, 1999.

[60] J. F. Salmon, "Predisposing factors for chronic-angle closure glaucoma," *Progressive Retinal Eye Research*, vol. 18, pp. 121-132, 1999.

[61] R. J. Casson and D. Franzco, "Anterior chamber depth and primary angle-closure glaucoma: an evolutionary perspective," *Clinic and Experimental Ophthalmology*, vol. 36, pp. 70-77, 2008.

[62] R. Ritch, "Argon laser treatment for medically unresponsive attacks of angle closure glaucoma," *American Journal of Ophthalmology*, vol. 94, pp. 97-204, 1982.

[63] D. H. Shin, "Argon laser iris photoagulation to relieve acute angle closure glaucoma," *American Journal of Ophthalmology*, vol. 93, pp. 348-350, 1982.

[64] M. W. Berns, R. S. Olson RS and D. E. Rounds, "In vitro production of chromosomal lesions with an argon laser microbeam," *Nature*, vol. 221, pp. 74, 1969.

[65] M. W. Berns, W. K. Cheng, A. D. Floyd, and Y. Ohnuki, "Chromosome lesions produced with an argon laser microbeam without dye sensitization," *Science*, vol. 171, pp. 903, 1971.

[66] C. B. Schaffer, N. Nishimura, E. N. Glezer, A. M. T. Kim and E. Mazur, "Dynamics of femtosecond laser-induced breakdown in water from femtoseocnds to microseconds," *Optical Express*, vol. 10, pp. 196-203, 2002.

[67] D. Du, X. Liu, G. Korn, J. Squier, and G. Mourou, "Laser induced breakdown by impact inonization in SiO2 with pulse widths from 7ns to 150 fs," *Applied Physics Letters*, vol. 64, pp. 3071-3073, 1994.

[68] F. Enguehard and L. Bertrand L, "Effects of optical penetration and laser pulse duration on laser generated longitudinal acoustic waves," *Journal of Applied Physics*, vol. 82, pp. 1532, 1997.

[69] A. Vogel, J. Noack, G. Hutterman and G. Paltauf, "Mechanisms of femtoseocond laser nanosurgery of cells and tissues," *Applied Physics B: Lasers and Optics*, vol. 81, pp. 1015-1047, 2005.

[70] H. P. Berlien, G. J. Muller, H. Breuer, N. Krasner, T. Okunata and D. Sliney, *Applied Laser Medicine*. Berline, Germany: Springer, 2003.

[71] M. K. George, J. W. Emerson, and S. A. Cheema, "Evaluation of a modified protocol for selective laser trabeculoplasty," *Journal of Glaucoma*, vol. 17, pp. 197-202, 2008.

[72] P. A. Quinto-Su and V. Venugopalan, "Mechanisms of laser cellular microsurgery," *Laser manipulation of cells and tissues*, vol. 82, pp. 113-151, 2007.

[73] A. J. Welch, "The thermal response of laser irradiated tissue," *IEEE Journal of Quantum Electronics*, vol. 20, pp. 633-644, 1984.

[74] F. Xu F, T. J. Lu, and K. A. Seffen, "Biothermomechanical behavior of skin tissue," *Acta Mechanica Sinica*, vol. 24, pp. 1-23, 2008.

[75] X. Liu, D. Du, and G. Mourou, "Laser ablation and micromachining with ultrashort laser pulses," *IEEE Journal of Quantum Electronics*, vol. 33, pp.1706-1716, 1997.

[76] J. G. Fujimoto, W. Z. Lin, E. P. Ippen, C. A. Puliafito, and R. F. Steinert, "Time-solved stiudies of Nd:YAG laser-induced breakdown," *Investigative Ophthalmology and Visual Science*, vol. 26, pp. 1771-1777, 1985.

[77] P. A. Barness and K. E. Rieckhoff, "Laser induced underwater sparks," *Applied Physics Letter*, vol. 13, pp. 282-282, 1968.

[78] B. Zysset, J. G. Fujumoto, and T. F. Deutsch, "Time resolved measurements of picosecond optical breakdown," *Applied Physics*, vol. 48, pp. 139-147, 1989.

[79] T Juhasz, X. H. Hu, L. Turi, and Z. Bor, "Dynamics of shock waves and cavitations generated by picosecond laser pulses in corneal tissue and water," *Lasers in Surgery and Medicine*, vol. 15, pp. 91-98, 1994.

[80] A. Vogel, M. R. Capon, M. N. Asyo-Vogel, and R. Birngruber, "Intraocular photodisruption with picosecond and nanosecond laser pulses: Tissue effects in cornea, lens and retina," *Investigative Ophthalmology and Visual Science*, vol. 35, pp. 3022-3044, 1994.

[81] T. Juhasz, F. H. Loesel, R. M. Kurtz, C. Horvath, J. F. Bille and G. Mourou, "Corneal Refractive Surgery with Femtoseond Lasers," *IEEE Journal of Selected Topics in Quantum Eelectronics*, vol. 5, pp. 902-910, 1999.

[82] G. Ku, and L. V. Wang, "Deeply penetrating photoacoustic tomography in biological tissues enhanced with an optical contrast agent," *Optics Letters*, vol. 30, pp. 507-508, 2005.

[83] Z. S. Sacks, “Femtosecond transscleral photodisruption for the treatment of glaucoma,” Ph.D dissertation, University of Michigan, 2000.

[84] Z. S. Sacks, R. M. Kurtz, T. Juhasz and G. A. Mourou, “High precision subsurface photodisruption in human sclera,” *Journal of Biomedical Optics*. vol. 3, pp.442-450, 2002.

CHAPTER 2

OUTFLOW RATE INCREASE BY A FEMTOSECOND LASER CREATED CHANNEL IN THE RABBIT EYES: *EX VIVO* EXPERIMENT

2.1. Introduction

As it was explained in glaucoma treatment section of Chapter 1, the advantage of the laser treatment is its incision free operation avoiding the structural damage and infection caused from scar and bleeding. However, compared to the surgical treatments creating extraordinary aqueous humor drainage**,** it can be expected that laser trabeculoplasty, which creates fine pores and induces biochemical change by thermal burning, would not have as much IOP reducing effect as the surgical treatments [1, 2]. In addition to this, it can be expected that thermal burns will be healed much quicker, leading to the limitation of longevity of laser treatment. Therefore, it should be a more complete treatment to create drainage channel by a laser without any incisional procedure, achieving the advantage of both treatments.

However, laser treatments could not be developed to create drainage channel due to the following technical difficulties; first, tissues should be disrupted with the minimal damage to the surrounding tissues. The multiple and intensive treatment by a high intensity laser over target space are needed to create channel, indicating the unavoidable

damage to tissues neighboring target space. Second, a laser beam should be focused beyond the target tissue. Drainage channel should be created from the posterior surface of sclera, especially trabecular meshwork, indicating the need of focusing a laser beam beyond the sclera. Third, the procedure to create the drainage channel should be developed. It takes a stronger treatment over the wider range of tissue to create the channel by the continuous disruption of tissues.

Recent studies proposed the potential of a femtosecond laser as an alternative to create the channel, making advantage of the changes in the properties of interaction with tissues over the reduction of pulse duration described in Chapter. 1. It was found that when the pulse duration is reduced to the femtosecond regime, the confined disruption of tissue can be obtained [3 - 5]. It was shown that a 1.7 μm wavelength tuned laser beam can be focused beyond the sclera, avoiding the big loss in energy while traversing the tissue [6]. It was also demonstrated that the transscleral channel can be created by scanning in a rectangular raster pattern from the posterior surface of the sclera [7].

In this chapter, the laser system to deliver a femtosecond laser will be introduced, followed by the experimental setup to mount the eye for the outflow measurement and the scanning. The outflow rate measurement setup to demonstrate the effect of drainage channel will be introduced also. Then, it will be described how the scanning was performed to create the designated pattern with predetermined parameters. Finally, the image of the channel and results of the outflow rate change measurements will be provided. These measurements demonstrate the efficiency of the subsurface partial thickness scleral channel created in cadaver rabbit eyes to increase the outflow rate, potentially leading to the reduction of IOP in the eyes of *in vivo* rabbits.

2.2. Methods

2.2.1. Experimental Setup

Laser and Beam Delivery System

The Ti:Sapphire laser system was composed of oscillator, pulse stretcher, regenerative amplifier, pulse compressor and optical parametric amplifier (Coherent; Santa Clara, CA) and arranged as shown in Figure 2.1. LabVIEW (National Instruments, Austin, TX) was used to develop the software to control the lasers. Amplified pulses with durations of 130-fs and pulse energies greater than 0.3 mJ were produced by the system at approximately 800 nm wavelength and 5 kHz repetition rate. The pulses from Ti:Sapphire laser system were tuned to 1.7 μm wavelength, by an optical parametric amplifier (Coherent; Santa Clara, CA). Output laser beam from optical parametric amplifier was expanded through beam expander, reflected by mirrors and focused to 5 μm diameter spot through 0.5 NA aspheric lens (Thorlabs; Newton, NJ)

Scanning Setup

A schematic view of the scanning mechanism is presented in Figure 2.2. The laser beam was focused into the tissue using a 0.5 NA focusing lens. The enucleated eyes were placed on a three-axis scanner stage driven by three stepper motors, one along each axis as described in Figure 2.3 (Newport MM1000 and stepper motors; Newport Corp., Irvine, CA). The stepper motors were controlled by a computer using LabVIEW 7.1 (National Instruments, Austin, TX) through electronic controller (ESP 300, Newport Corp., Irvine, CA). The axis parallel to the propagation of the light is referred to as the Z-axis. The X-axis is tangential to the corneal perimeter and the Y-axis is perpendicular to the XZ plane. As a result, the three scanning axes compose a Cartesian coordinate system. In order to

minimize light scattering on the surface of the tissue a microscope slide was placed on the cadaver eye at the proposed location of the channel. The scanner stages were moved along programmed patterns with predetermined parameters to create the partial thickness AH drainage channel in the sclera.

Outflow Rate Measurements

Standard perfusion experiments were performed in cadaver rabbit eyes to demonstrate the effect of subsurface partial thickness scleral channel created by the femtosecond laser and investigate the effect of channel dimensions on the extent of the channel effect. Figure 2.4 displays the schematics of the aqueous humor outflow measurement setup modified from the one developed by Brubaker [8]. The reservoir containing balanced salt solution (BSS) was connected to the enucleated rabbit eye. A 23 gauge needle with an opening 5 mm from the tip was inserted into the eye in the holder so that the tip was located in the posterior chamber and the hole in anterior chamber, to prevent the deepening of anterior chamber. The position of needle and eye in the holder was fixed in gypsum. The surface of eye was covered with wet paper to prevent dehydration. A valve was introduced between needle and tube to detach and reattach the eye to the outflow measurement setup for the laser treatment. The intraocular pressure (IOP) was controlled by adjusting the height difference between the surface of the liquid in reservoir and the tip of needle. The mass of liquid in reservoir was measured periodically by a micro scale connected electronically to a computer using LabVIEW 7.1 (National Instruments, Austin, TX).

2.2.2. Experimental Procedures

Enucleated rabbit eyes no older than 48 hours postmortem were used in the studies. As the first step, aqueous outflow rate was established in an untreated eye. This step is referred to as the baseline measurement and was conducted in the following order:

1. The perfusion needle was inserted into the eye as the above described procedure and position, preventing the introduction of bubble into the anterior chamber. Then the eye and the needle were incased in gypsum.
2. The flow was started by opening the valve between the reservoir and the eye, and the flow rate was stabilized by leaving the eye setup intact for 30 minutes at 10 mmHg perfusion pressure.
3. The perfusion pressure, also the IOP in this setup, was set to 15 mmHg by adjusting the height difference between the surface of solution in reservoir and the eye globe.
4. The change of mass of the reservoir was measured every 5 second for 10 minutes by the micro scale connected to the computer.
5. Steps 3, 4 were repeated at 25mmHg perfusion pressure.

Flow rates were measured in the unit of mass/time and converted into volume/time (µl/min) by taking into account of the density of the BSS solution in the reservoir. The flow rate was selected as the steady state outflow rate that kept same value for at least 2 min. The valve was closed after the baseline measurement, and the eye and needle contained in the holder were detached from the outflow measurement setup.

A microscope slide was placed on the globe at the position where the channel needed to be created, and the eye was placed on the scanner stage. Laser pulse energy

was set to 17μJ. To determine the zero depth (reference point for the scanning in the Z direction), the focal point of laser beam was adjusted to the bottom surface of the applanation glass (anterior scleral surface). Before starting the scanning process the focal point of the laser was moved into sclera, so that the optical breakdown occurred at or below the posterior scleral surface. Scanning parameters were set to be a 3 μm spot separation, a 5 μm line separation and a 2 μm layer separation. Spot separation was set by adjusting the scanning velocity along X axis and line, layer separations were entered into LabVIEW program as an input. As shown in Figure 2.2, scanning along X and Y axis is made on the surface normal to the direction of beam propagation.

As described in Figure 2.5, the focal point of the laser was scanned along a raster pattern so that the focus of the laser is moved parallel to the width of the channel by the spot separation (a predetermined channel dimension), and moved, by a line separation, normal to the previous movement. Then, focus was moved parallel to the last movement along width in the opposite direction and moved by a line separation. These movements were repeated until the sum of the moving distance along the line separation became equal to the length, another predetermined channel dimension. Then, the focus was moved up along Z by a layer separation and the scanning started over another layer in the opposite direction to the previous layer. The scanning stopped before the top surface of channel reached the anterior surface of the sclera to preserve the layer between these two surfaces. After finishing the creation of the partial thickness drainage channel, the eye was reconnected to the outflow measurement setup. The outflow rate was measured following the outflow measurement protocol described above. Then, the shape of channel was monitored with OCT image to evaluate the efficiency of channel creation.

The above procedure was repeated on 3 eyes, creating the channels in different dimensions, 800μm (width) × 320μm (length), 800μm (width) × 240μm (length) and 800μm (width) × 180μm (length), to demonstrate the effect of channel dimensions on the amount of the increased outflow rate.

2.3. Results

Figure 2.6 shows that a partial thickness drainage channel was created at the angle of the iris and cornea as bordered by yellow line. It can be seen that the scan was made so that the thin layer was remained between the top of channel and the surface of the sclera.

Experimental data were obtained from 3 enucleated rabbit eyes to compare the effects of channel with different dimensions, 800μm (width) × 320μm (length), 800μm (width) × 240μm (length) and 800μm (width) × 180μm (length), corresponding to cross sectional areas of 0.144, 0.192 and 0.256 mm^2. In each eye, the channel was created following the same procedure in the same parameters except the dimensions, width and length, of the eye.

As it can be seen in Figure 2.7, the outflow rate was increased in every eye, demonstrating the outflow increasing effect of the channel. In addition to this, it is obvious that the amount of the increased outflow rate after the laser treatment is increased in a positive relation with the width of the channel, indicating that the amount of the increased outflow rate can be controlled by adjusting the dimension of channel. This increase is considerably larger than any washout effect measured in cadaver eye perfusion experiments in various species [9] and in the eyes of *in vivo* rabbits [10].

Therefore, it can be concluded that most of the outflow rate increasing effect is from the subsurface channel.

2.4. Discussion

It was demonstrated that the subsurface channel can be created by a femtosecond laser [7]. However, the subsurface channel must be created at the optimal position in the sclera of the eye to show the potential of a femtosecond laser as a laser for the eye treatment. Therefore, the first goal of this study is to demonstrate that the subsurface channel can be created at the designated position in the sclera of *ex vivo* rabbit eye for the treatment, because the channel was created in the piece of dehydrated sclera in the previous study [7].

Another goal of this study is to demonstrate the outflow rate increasing effect and the potnetial of the subsurface channel that the outflow rate increase can be controlled by the channel dimensions, because, assuming the IOP increase by the increased outflow resistance, the controllable outflow rate increase means that IOP can be controlled to be reduced into the normal range. Figure 2.8 shows the increased outflow rate at 25 mmHg over the channel dimensions to mimic elevated IOP in glaucomatous eyes, demonstrating the potential of the control of reduced IOP by adjusting the channel dimensions.

OCT was used to monitor the location and shape of channel, because it is advantageous to see the intact channel. There are other methods that can monitor the section of tissue by slicing it after the fixation. However, our experiment focused on the shape of channel remaining only 10 % of sclera thickness and it is very significant to save the shape of channel that is difficult to save by the tissue cutting methods. The existing

methods that fix the tissue are efficient in saving the overall shape of the tissue. However, taking into account the remaining layer of 10% of the original thickness, the subsurface tissue can't be fixed strong enough to save the shape of channel through the cutting process. The reliability of the subsurface image of OCT might be questioned, because it is a subsurface channel. However, the thickness of sclera is less than 0.5 mm [11] and, taking into account the papers on the reliability of OCT images of the intraocular structure [12 - 14], it can be concluded that the OCT image is reliable enough to provide the valuable monitoring information on the shape and location of channel.

This experiment indicates that a femtosecond laser treatment has high potential to decrease IOP under in vivo rabbit eyes. To prove this, we conducted in vivo rabbit treatment to be discussed in Chapter 4.

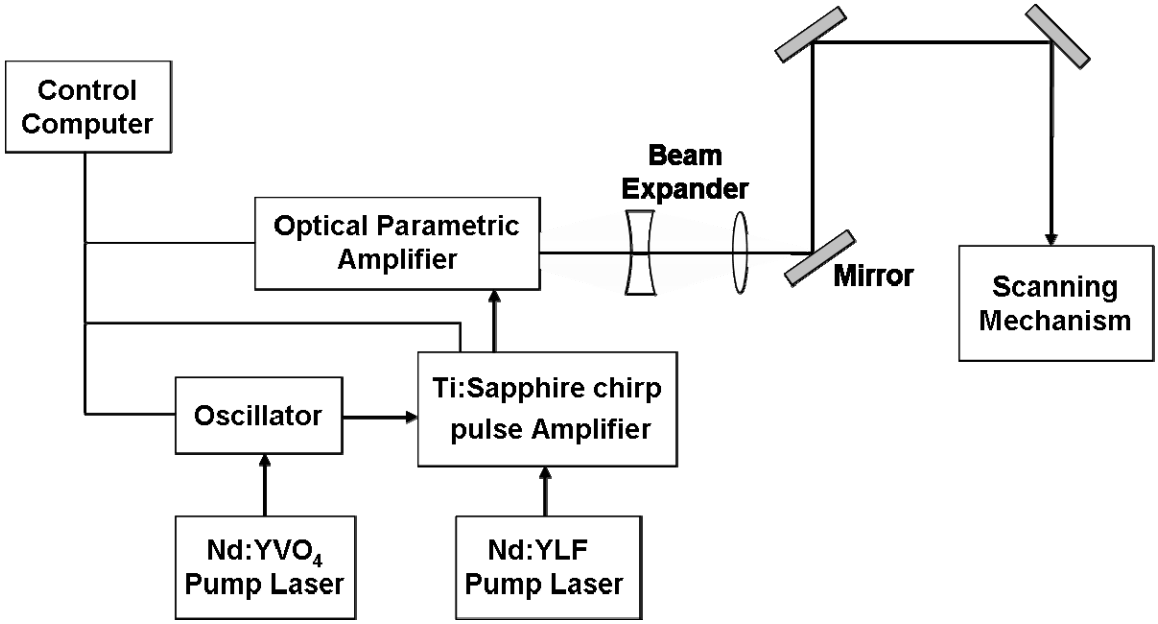

Figure 2.1. Overall laser delivery system.

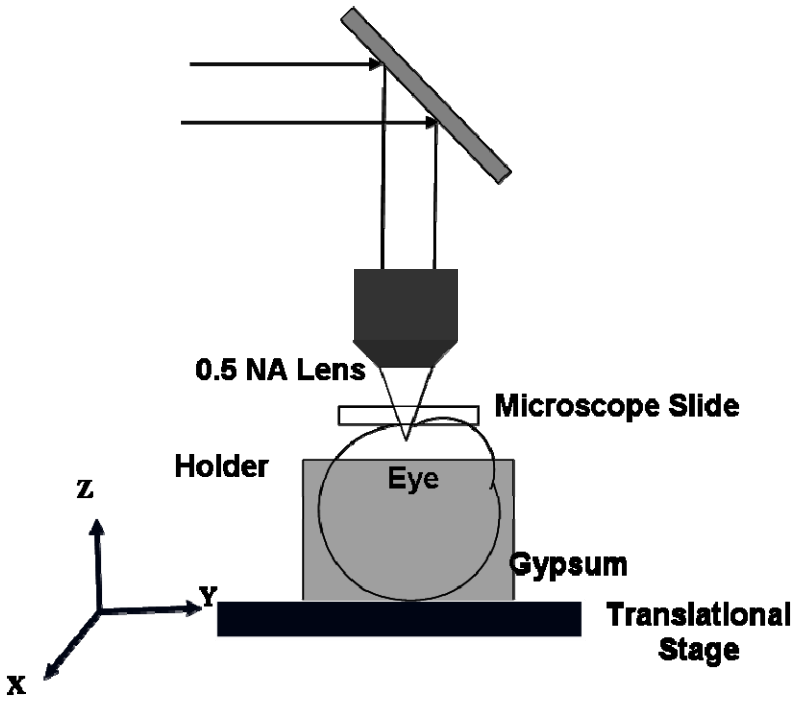

Figure 2.2. The scanning mechanism.

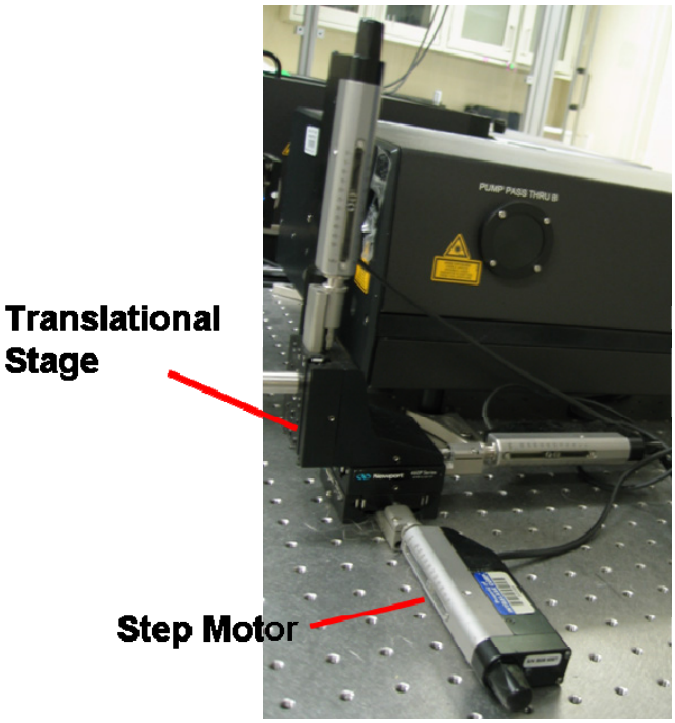

Figure 2.3. The translational stage used in the experiment.

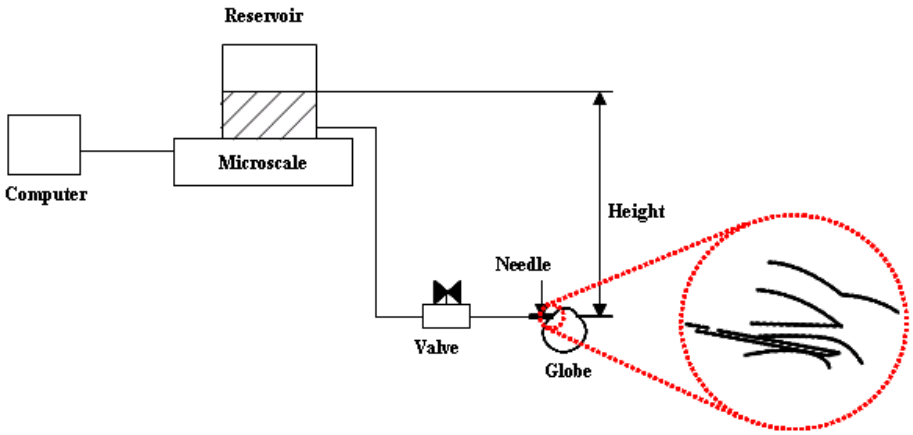

Figure 2.4. Outflow rate measurement setup.

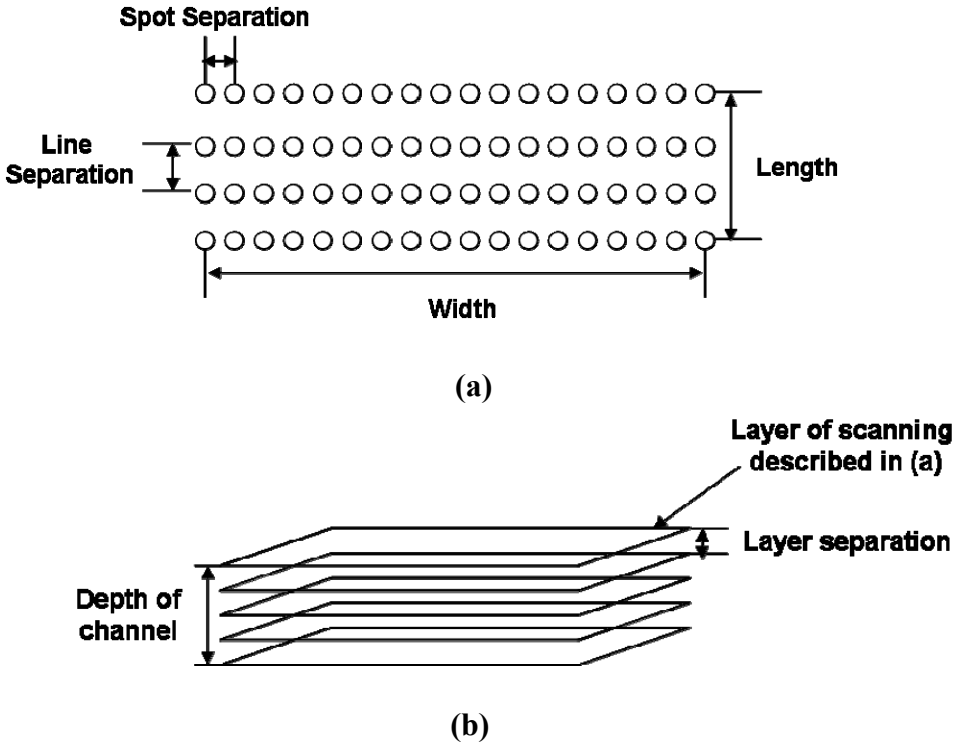

Figure 2.5. (a) Scanning over one layer. (b) Scanning of layers to create channel in predetermined depth

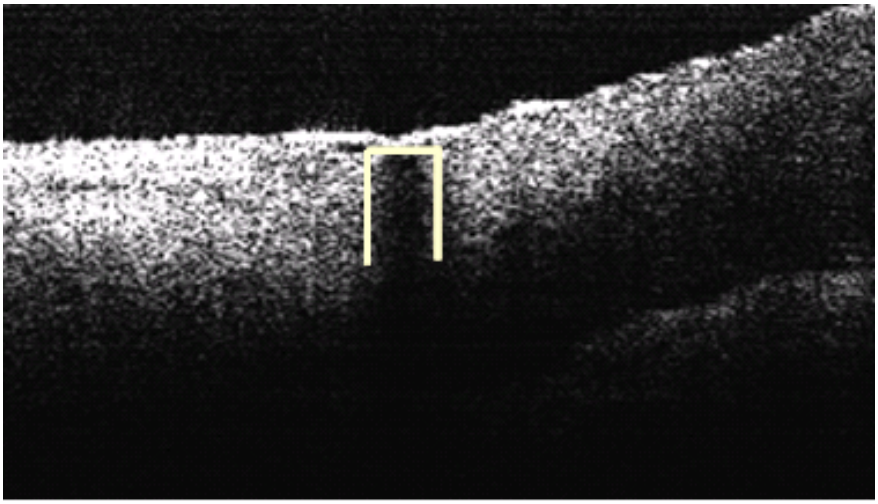

Figure 2.6. Subscleral channel at the angle of the eye (yellow line).

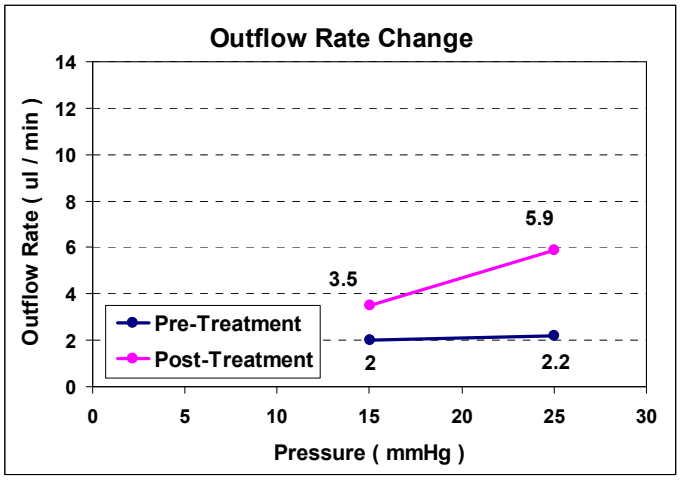

(a)

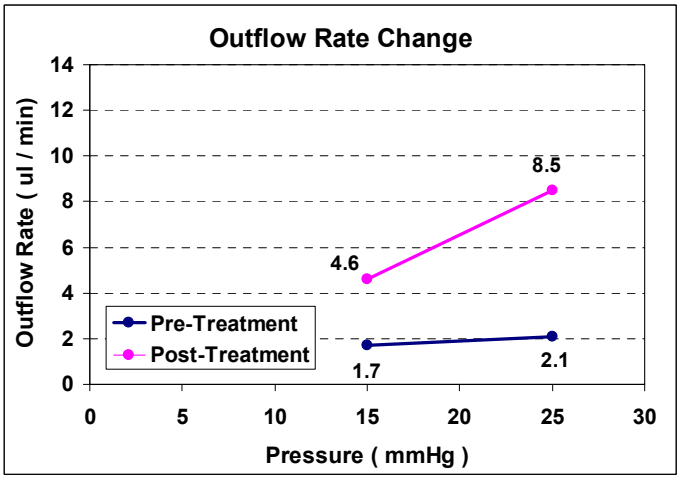

(b)

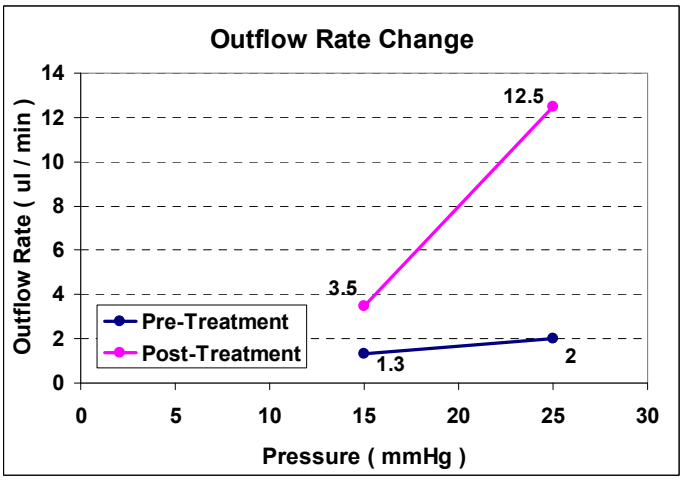

(c)

Figure 2.7. Outflow rate increase in each eye with channel in different dimension (μm) ((a) 800 × 180, (b) 800 × 240, (c) 800 × 320).

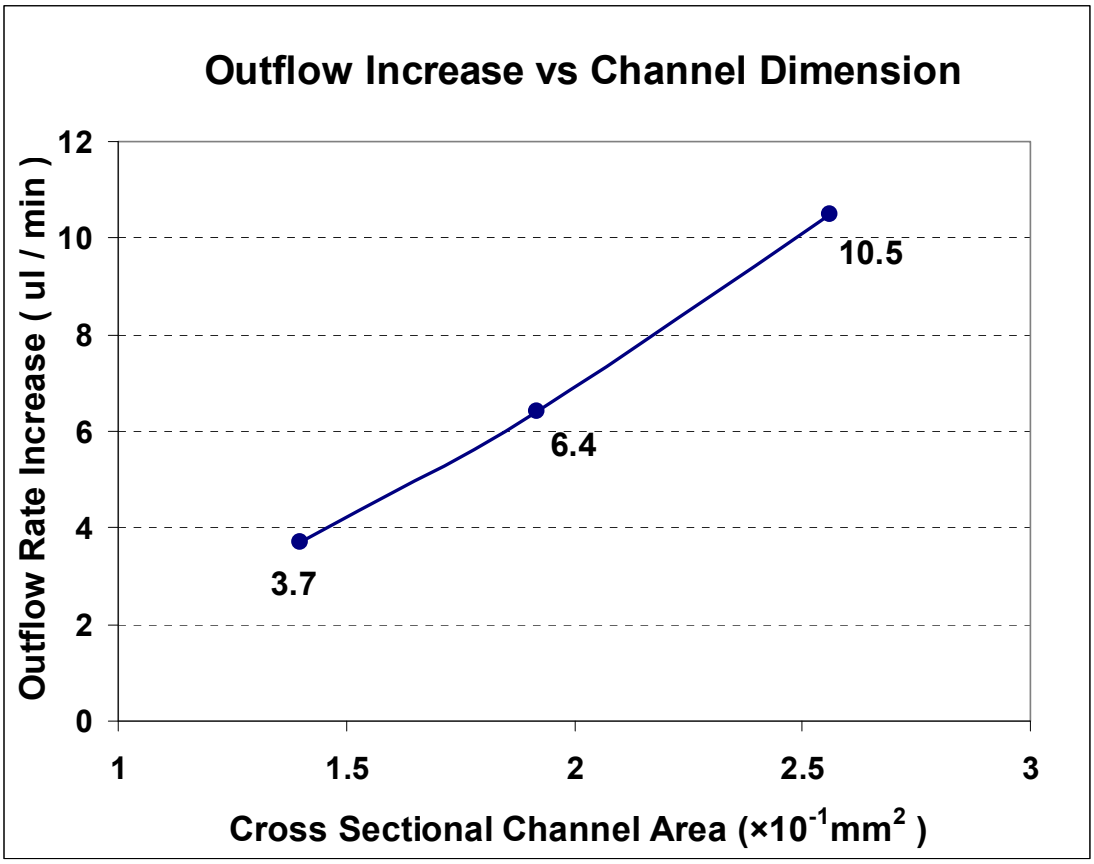

Figure 2.8. Outflow rate increase at 25 mmHg in each channel.

2.5. References

[1] J. C. Morrison and I. P. Pollack, *Glaucoma: Science and Practice*. New York: Thieme Medical Publishers, 2003.

[2] J. V. Thomas, C. V. Belcher III, and R. J. Simmons. *Glaucoma Surgery*. St. Louis: Mosby Year Book, 1992.

[3] T. Juhasz, G. A. Kastis, C. Suarez, Z. Bor, and W. E. Bron, "Time-resolved observations of shock waves and cavitation bubbles generated by femtosecond laser pulses in corneal tissue and water," *Lasers in Surgery and Medicine*, vol. 19, pp.23-31, 1996.

[4] W. Kautek, S. Mitterer, J. Kru¨ger, W. Husinsky, and G. Grabner, "Femtosecond-pulse laser ablation of human corneas," *Applied Physics. A-Materials Science & Processing*, vol. 58, pp. 513-518, 1994.

[5] D. Du, J. Squier, R. Kurtz, V. Elner, X. Liu, G. Guttmann, and G. Mourou, *Damage threshold as a function of pulse duration in biological tissue*. New York: Springer-Verlag, 1994.

[6] Z. S. Sacks, R. M. Kurtz, T. Juhasz, G. Spooner, and G. A. Mourou, "Subsurface photodisruption in human sclera: wavelength dependence," *Ophthalmic Surgery Lasers & Imaging*, vol. 34, pp. 104-114, 2003.

[7] Z. S. Sacks, R. M. Kurtz, T. Juhasz, and G. A. Mourou, "High precision subsurface photodisruption in human sclera," *Journal of Biomedical Optics*, vol. 7, pp. 442-450, 2002.

[8] R. F. Brubaker, "The effect of intraocular pressure on conventional outflow resistance in the enucleated human eye," *Investigative Ophthalmology & Visual Science*, vol. 14, pp. 286- 292, 1975.

[9] K. Erickson-Lamy, A. M. Schroeder, S. Bassett-Chu, and D. L. Epstein, "Absence of time-dependent facility increase (washout) in the perfused enucleated human eye," *Investigative Ophthalmology & Visual Science*, vol. 31, pp. 2384-2388, 1990.

[10] J. B. Ruben, R. A. Moses, and W. J. Grodzki, "Perfusion Outflow Facility in the Rabbit Eye," *Invest Ophthalmology & Visual Science*, vol. 26, pp.153-158, 1990.

[11] J. H. Prince, *The rabbit in the eye research*. Springfield, IL: C. C. Thomas, 1964.

[12] M. Wojtkowski and A. F. Kowalczyk, "Full range complex spectral optical coherence tomography technique," *Optics Letters*, vol. 27, pp. 1415-1417, 2002.

[13] C. Wirbelauer, A. Karandish, H. Aurich, and D. T. Pham, "Imaging scleral expansion bands for presbyopia with optical coherence tomography," *Journal of Cataract Refractive Surgery*, vol. 29, pp. 2435-2438, 2003.

[14] S. Radhakrishnan, J. Goldsmith, D. Huang, V. Westphal, D. K. Dueker, A. M. Rollins, J. A. Izatt, and S. D. Smith, "Comparison of Optical Coherence Tomograpgy and Ultrasound Biomicroscopy for Detection of Narrow Anterior Chamber Angles," *Archive of Ophthalmology*, vol. 123, pp. 1053-1059, 2005.

CHAPTER 3

FINITE ELEMENT MODEL TO PREDICT IOP REDUCED BY A FEMTOSECOND LASER CREATED CHANNEL

3.1. Introduction

The purpose of glaucoma treatment is to reduce the elevated IOP, but if IOP is not reduced into the normal range, the continuous treatment is needed until the reduced IOP reaches the normal range. Therefore, the initiate treatment is significant so that IOP can be reduced into the normal range quickly. The first step should be to predict the exact result of the treatment. Especially for the surgical treatment, it is expected that the mathematical model has the potential to not only predict the reduced IOP but propose the optimal treatment.

There have been a number of efforts to model AH dynamics [1-3], but most have focused on qualitative aspects of AH flow patterns [2] or the relationship between IOP and changes in ocular structures [1, 3]. They have also relied on 2D models, without comparison to experimental data. There have been efforts to model the permeability of the sclera [4]. However, they focused on the model of piece of sclera, not under *ex vivo* or *in vivo* condition of the entire eye globe and AH production and drainage system that can predict the actual IOP. In contrast to these studies, 3D mathematical model for AH flow

in the rabbit eye was constructed that has the potential to predict IOP compared to the proper experimental data. In this chapter, the process of developing 2D model into 3D model will be described and it will be assessed the feasibility of predicting IOP with a 3D mathematical model and its potential use as a tool in predetermining the dimensions of the partial thickness channel to reduce IOP predictably in glaucoma management.

3.2. Basic Assumptions

A 2D finite element model was developed and expanded to 3D model to simulate the AH flow dynamics in rabbit eyes based on the following assumptions:

1. The amount of AH flowing out of the rabbit eye through the uveoscleral pathway is not exactly known and the uveosceral flow is not changed over increased IOP [5]. Therefore, it is assumed that all the AH outflow occurs through the trabecular pathway.
2. There is no available episcleral vein in *ex vivo* cadaver rabbit eye. Therefore, it is assumed that AH flows through the limbus, the intermediated zone between corneal and sclera, to below the conjunctiva.
3. The trabecular pathway in the rabbit eye is porous, so that outflow through the pathway follows the Brinkman equation and its resistance to the outflow can be characterized with permeability in the equation. This assumption is in line with the efforts to quantify the outflow resistance [2], and ultimately to provide the prediction of the decrease in IOP.

4. The resistance of pathway is characterized with one comprehensive permeability value rather than a summation of the permeability of each component of the pathway.

5. The structures of the eye such as the cornea are rigid materials, and it is assumed that all structural components such as lens and iris inside the eye do not move with changes in IOP. The relationship between IOP and movement of eye structures has been investigated [1], but it is not the focus of the current study.

6. The potential impact of temperature and circulatory perfusion on the AH outflow was not considered. It was assumed that the fluid flowing into the eye from the reservoir as well as the eye is equilibrated to room temperature. Previous studies demonstrated [2] that there are two potential heat sources that can have impact on AH flow, the temperature difference between the cornea and the rest of the eye and temperature differences created by the blood flow. These temperature gradients can affect the pattern of AH flow, but its effect on IOP and the increased flow rate through the channel is expected to be ignorable.

3.3. Geometry of Model

The overall dynamics of AH dynamics in rabbit eye is very similar to the human eye in that it is secreted from ciliary body and exits the eye in the same pathway as humans except the absence of Schlemm's canal, scleral spur [2, 6]. These are structural differences inside the pathway that can be ignored in modeling based on the assumptions proposed in the previous section. Therefore, basic 2D model could be constructed, as shown in Figure 3.1, so that it focused on AH flow dynamics [7] in the anterior chamber. It was shown that the gap between the lens and iris is on the order of micrometers [3, 8].

This very narrow gap is difficult to mesh and even if it is meshed, it cannot be calculated with reliable convergence and stability, especially in the 3D model without the use of a supercomputer. Therefore, our model focused on AH dynamics after it entered the anterior chamber, passing by the gap. The anterior chamber was modeled as a hemisphere with a diameter of 12mm along the edge of the iris [2]. The height of the trabecular meshwork, the length from the edge of iris to the Schwalbe's line, in human eyes ranges from 0.38 mm to 0.86 mm and the average is 0.65 mm [9]. Therefore, the trabecular meshwork (TM) in rabbit eye was assumed to have a height of 0.45 mm, lower than human eye. In order to simplify the model, the AH inflow was assumed to enter anterior chamber through the velocity inlet marked with a red line in Figure 3.1. Similar simplification approaches to model AH in the anterior chamber has been qualitatively tried [2]. The 3D model was developed by the revolution of the modified axially symmetric 2D model by 360^{o}. The geometry of 3D model with the femtosecond laser created channel (marked with a circle) is shown in Figure 3.2.

The channel was created in the 3D model so that the remaining layer between the top of channel and anterior surface of sclera is thin, as described in Figure 3.3(b), but it still provides some resistance, characterized with the modified permeability to be referred to as "effective channel permeability", to the outflow.

3.4. Governing Equations and Boundary Conditions

The Navier-Stokes equation governing AH flow in the anterior chamber and the continuity equation are presented as [10],

$$\rho\left(\frac{\partial \mathbf{u}}{\partial t}+\mathbf{u}\cdot\nabla\mathbf{u}\right)-\nabla\cdot\left[\eta\left(\nabla\mathbf{u}+(\nabla\mathbf{u})^{T}\right)\right]+\nabla\boldsymbol{P}=\mathbf{F} \quad \textbf{(1)}$$

$$\frac{\partial\rho}{\partial t}+\nabla\cdot(\rho\mathbf{u})=0 \quad \textbf{(2)}$$

This model is on the AH flow in the steady state and the equations can be modified to the following,

$$\rho\mathbf{u}\cdot\nabla\mathbf{u}-\nabla\cdot\left[\eta\left(\nabla\mathbf{u}+(\nabla\mathbf{u})^{T}\right)\right]+\nabla\boldsymbol{P}=0 \quad \textbf{(3)}$$

$$\nabla\cdot\mathbf{u}=0 \quad \textbf{(4)}$$

The AH flow through trabecular meshwork that can be modeled as a porous media is governed by Brinkman equation,

$$\left(\frac{\rho}{\varepsilon}\right)\frac{\partial\mathbf{u}}{\partial t}-\nabla\cdot\left[\frac{\eta}{\varepsilon}\left(\nabla\mathbf{u}+(\nabla\mathbf{u})^{T}\right)\right]+\nabla\boldsymbol{P}+\frac{\eta}{\kappa}\mathbf{u}=\mathbf{F} \quad \textbf{(5)}$$

$$\frac{\partial\rho}{\partial t}+\nabla\cdot(\rho\mathbf{u})=0 \quad \textbf{(6)}$$

This equation also can be modified for the steady state flow to

$$-\nabla\cdot\left[\frac{\eta}{\varepsilon}\left(\nabla\mathbf{u}+(\nabla\mathbf{u})^{T}\right)\right]+\nabla\boldsymbol{P}+\frac{\eta}{\kappa}\mathbf{u}=0 \quad \textbf{(7)}$$

$$\nabla\cdot\mathbf{u}=0 \quad \textbf{(8)}$$

where $\mathbf{u}$ is velocity (m/s), ρ is density (kg/m^3), η is dynamic viscosity (Pa · s), **F** is volume force, P is pressure and κ is permeability (m^2). Each equation was modified, because we focused on the steady state flow in anterior chamber to get the permeability and the volume force is not included**.** In Brinkman equation, the effect of inertial loss

term, the first tem of equation (7), is expected to be ignorable, considering the velocity of the AH flow in μl / min. However, this term was included in effort to integrate the whole effect. The properties of AH used in model were $\rho = 1000\ kg/m^3$, $\eta = 1.002 \times 10^{-3}$ Pa ·s. The permeability of pathway is calculated by fitting the experimental AH outflow data measured in untreated enucleated rabbit eyes introduced in Chapter 2 to the 2D model.

Boundary conditions at velocity inlet were given so that the inflow rate was the same as the one measured in the experiment of Chapter 2. This eliminates the problems from meshing the narrow iris-lens gap. (see Figure 3.1 and 3.4). In the eye of in vivo rabbit, AH flows into episcleral vein to exit the eye. Therefore, the final destination of AH flow should be modeled to be the constant pressure boundary condition, 9.6 mmHg, the pressure in the episcleral vein [11]. However, there is no available blood pressure in the episcleral vein in cadaver eyes and the boundary condition was given as atmospheric pressure based on the basic assumption 2 and additional assumption that the pressure difference between the posterior surface of conjunctiva and the air should be ignorable.

3.5. Numerical Methodology

Finite element mesh were generated for 2D as shown in Figure 3.4 and refined until the IOP value became independent of meshes. The velocity was assigned to the red marked line in Figure 3.1 so that the inflow over that line is equal to the inflow rate before the laser treatment at 25 mmHg in each eye from the experiment data from Chapter 2. The different permeability values of trabecualr pathway were continuously fitted until 25 mmHg IOP were calculated.

3D model was developed to simulate the AH flow in the eye with a femtosecond laser created channel. A huge number of meshes are needed to develop complete 3D model for AH fluid in the anterior chamber and it takes the huge computational ability such as supercomputer or workstation to calculate the equations. There was no available access to computational equipment. Therefore, 3D model was developed in the way that can get the utmost out of the available computation capacity. Geometry of 3D model was developed, as shown in Figure 3.2, meshed and the same boundary condition was given as 2D model.

The governing equations were discretized and solved by COMSOL Multiphysics 3.4. Equations were solved by an affine invariant form of the damped Newton method [10]. In each Newton step, GMRES method was used with incomplete LU preconditioner.

3.6. Calculation Procedure

AH should be simulated in 3D model and the permeability values of pathways should be known to predict the effect of the subscleral drainage channel on IOP. Therefore, the overall calculation was processed in the following order.

3.6.1. Calculation of Permeability Values of Untreated Pathway in 2D Model

The inflow rates in the untreated eyes before the laser treatment were assigned into 2D model to calculate the permeability values of the untreated pathway by continuously fitting the different values until IOP was calculated to be 25 mmHg.

3.6.2. Verification of the Model Expansion to 3D

The 2D model was expanded to 3D by the revolution by 360 degree. The ideal model expansion is to simulate AH in 3D model in the same flow pattern and IOP as in

2D model under the same input and boundary conditions. The flow pattern and IOP values in 3D model were compared to those in 2D model to verify the reliability of expanded 3D model.

3.6.3. Calculation of Permeability of the Remaining Layer

The permeability of the remaining layer between the top of channel and the anterior surface of sclera was calculated by continuously fitting the permeability values to the layer under the calculated permeability values of untreated pathway and boundary conditions from the experimental data of the post-treatment outflow rate until IOP was calculated to be 25 mmHg in each eye.

3.7. Results

AH flow in the intact was simulated by 2D model as shown in Figure 3.5 in the same pattern as predicted in other papers [3], qualitatively verifying the model. Permeability values of the trabecular meshwork in 2D model were calculated to be 1.34×10^{-14}, 1.28×10^{-14}, 1.25×10^{-14} m^2 in the ascending order of channel dimensions of 800 μm × 180 μm, 800 μm × 240 μm and 800 μm × 320 μm, corresponding to cross sectional areas of 0.144, 0.192 and 0.256 mm^2.

The agreement with 2D model was 95 %, 96 %, 98 % and the flow pattern in 3D was predicted in the same pattern as in 2D model as described in Figure 3.6. Figure 3.7 also shows the flow through the channel. Considering the ultimate goal of the model is to predict IOP based on the provided information, the outflow rate, it can be concluded that the reliable value of IOP can be predicted by 3D model.

The effective channel permeability of each eye was calculated to be 3.2×10^{-13} m^2, 4.35×10^{-13} m^2 and 5.15×10^{-13} m^2 in the ascending order of channel dimensions.

3.8. Discussion

The goal of this modeling is to demonstrate the potential of 3D FEM model as a tool that can predict the reduced IOP by simulating AH. Modeling the outflow in enucleated cadaver eyes provided challenge for this study. Since there is no blood flow in the episcleral vein, the boundary condition for final destination of AH could not be used in the model. To describe outflow in the enucleated rabbit eyes, we assumed that AH flows through the pathway to the posterior surface of the conjunctiva, therefore boundary conditions were set to the atmospheric pressure rather than the episcleral vein pressure. However, this is reasonable assumption, because, taking into account the location of the episcleral vein just below the conjnuctiva [11] and porosity of the remaining layer beyond the episcleral vein, it can be expected that AH would continuously flow beyond the episcleral vein.

Uveoscleral flow was neglected in the model, because its exact flow rate is not known and its contribution to the total outflow is reduced as IOP is increased as mentioned in introduction [12]. This assumption is not expected to result in considerable errors in the model as we focused on modeling the effect of the partial thickness drainage channel on the outflow dynamics through the trabecular pathway.

The effect of partial thickness drainage channel was modeled by assigning appropriate permeability value for the remaining thin scleral layer at the anterior end of the channel. It could be shown that the amount of increased outflow rate is in positive

relation with the permeability values of the effective channel permeability. It means that the amount of IOP reduction is affected also by the value of the effective channel permeability. Therefore, it can be concluded that it is necessary to know the value of the effective channel permeability to predict IOP. The effective channel permeability should have the thickness dependent value and it can be calculated by creating very small channel with the thickness that the actual channel will have and inputting the amount of IOP reduction by this small channel, the measured inflow rate into the model developed in this study. Then, IOP can be predicted by 3D model and the optimal dimension of channel can be proposed to reduce IOP as much as needed.

Necessity of 3D Model

There might be the potential question on the need or necessity of 3D model to predict IOP if the channel effective channel permeability defines IOP reducing efficiency of channel. The necessity of channel can be demonstrated by introducing the factor of safety (FOS) used in design [13]. If FOS is 1, it means the design is optimized just as much as needed. Applying this concept to this treatment, if channel is created just in the calculated dimensions, it means that the channel has been created based on the assumption of no change in the properties of the eye and excluding any unexpected accident on the eye. Therefore, the possible unexpected changes such as additional IOP elevation or impact to the eye should be taken into account when the dimension and location of channel are decided. In this study, the channel was created so that only thin layer was remained to magnify the effect. However, if this treatment is employed in the clinical purpose, the location and dimension of channel should be determined so that the treatment must be able to stand against unexpected changes. One of the possible ways is to adjust the

channel dimensions by increasing the thickness of the remaining layer. Its effect can be made up by increasing width and length or creating multiple channels can be another way. In these cases, the necessity of 3D model can be demonstrated by investigating the change of ratio of the flow through the top surface of channel, described in Figure 3.3(b) and 3.7(b), to whole outflow over different depth.

Figure 3.8 shows that the ratio of the flow through the top surface of channel is decreased with the increase of the thickness of the remaining layer. It means the effect of the flow through the trabecular pathway excluding the remaining layer is increased. Ultimately, it demonstrates the necessity of 3D model to predict IOP, taking into account the effect of these flows.

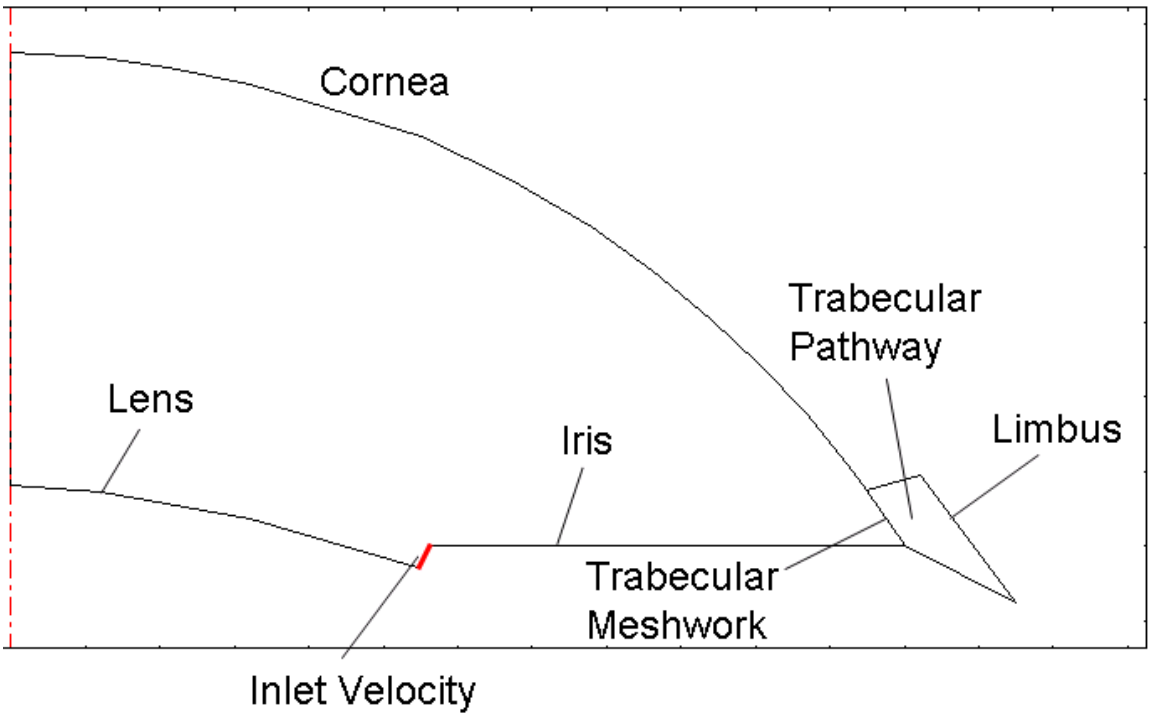

Figure 3.1. The simplified 2D model.

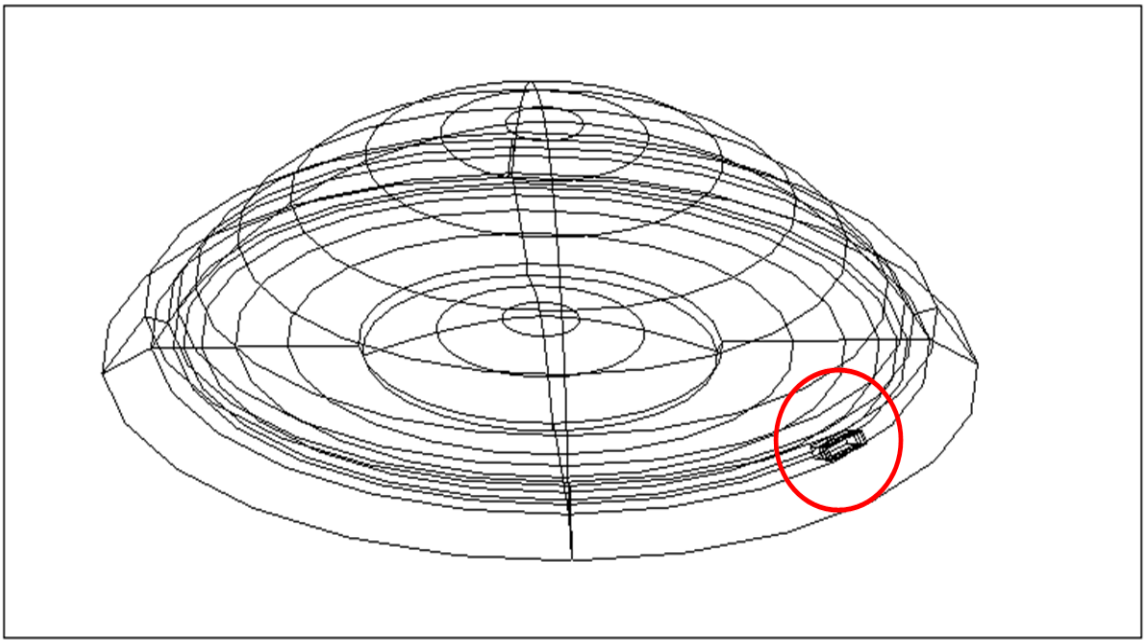

Figure 3.2. The geometry of 3D model and the channel created by a femtosecond laser.

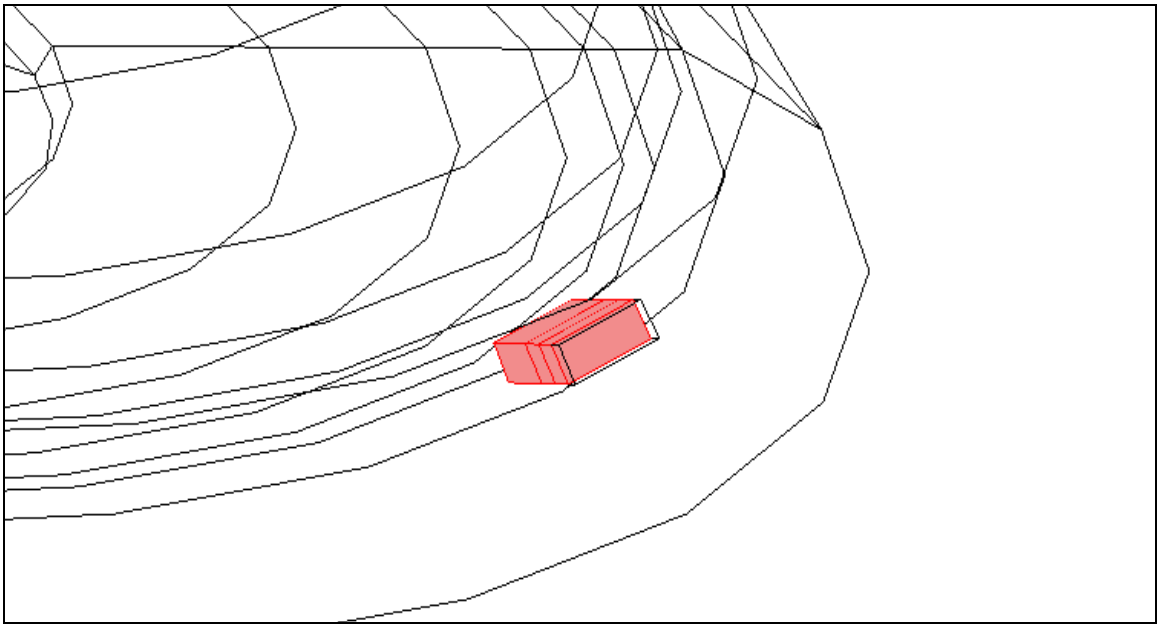

(a)

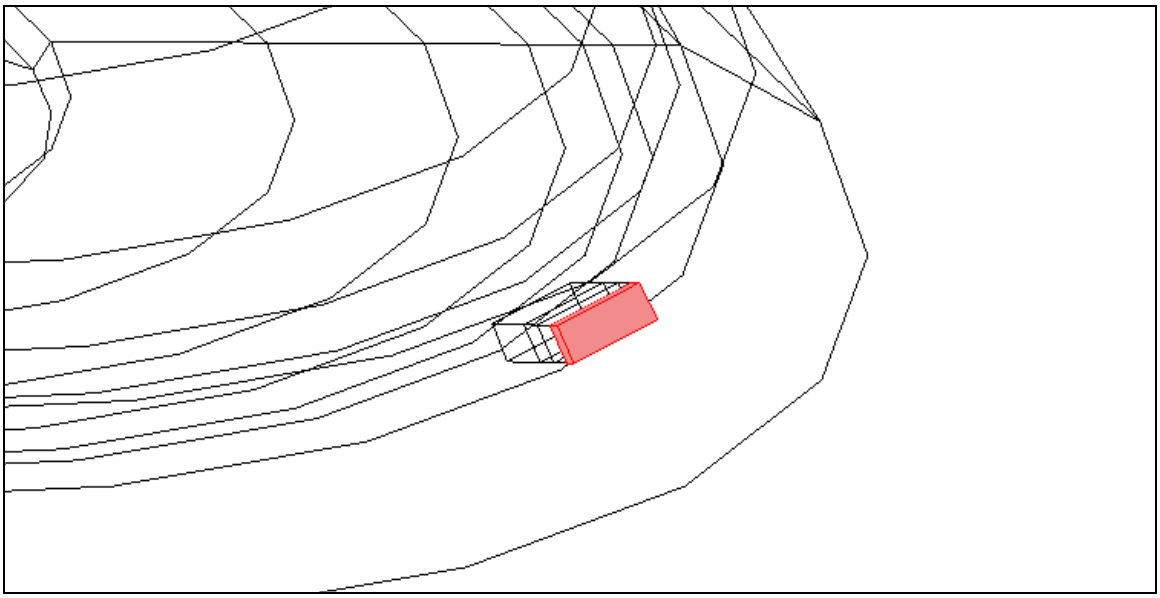

(b)

Figure 3.3. Details of 3D model corresponding to (a) Subsurface channel (highlighted with red) and (b) Thin layer with effective channel permeability (highlighted with red).

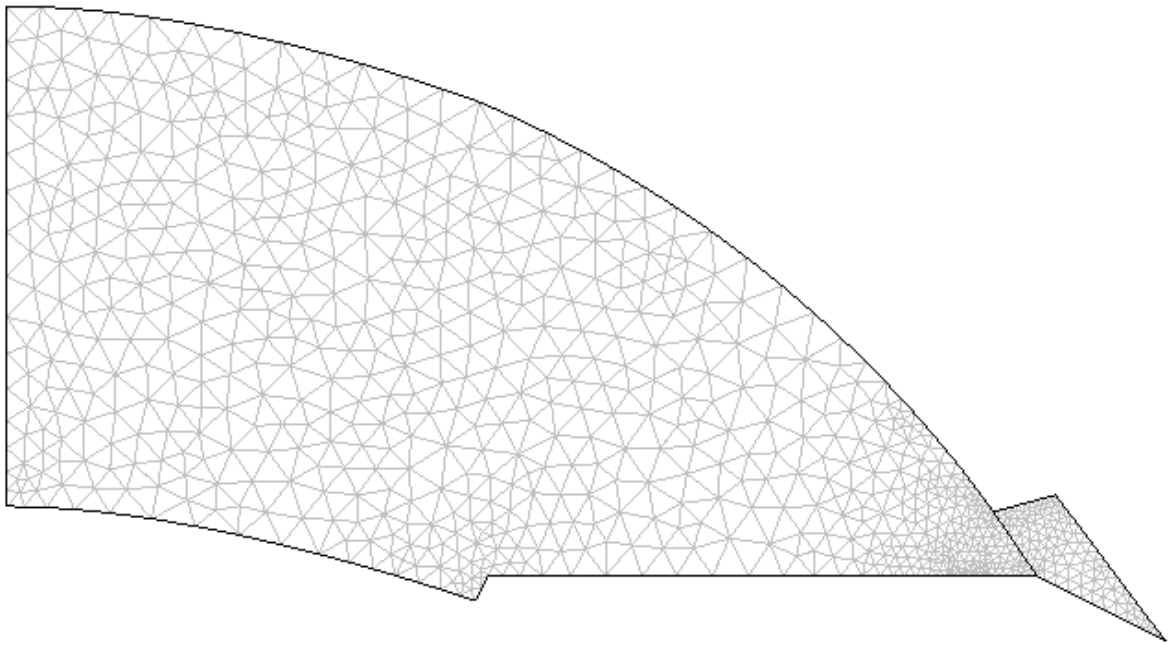

Figure 3.4. The mesh used in the 2D model.

Figure 3.5. The AH flow predicted by the 2D model.

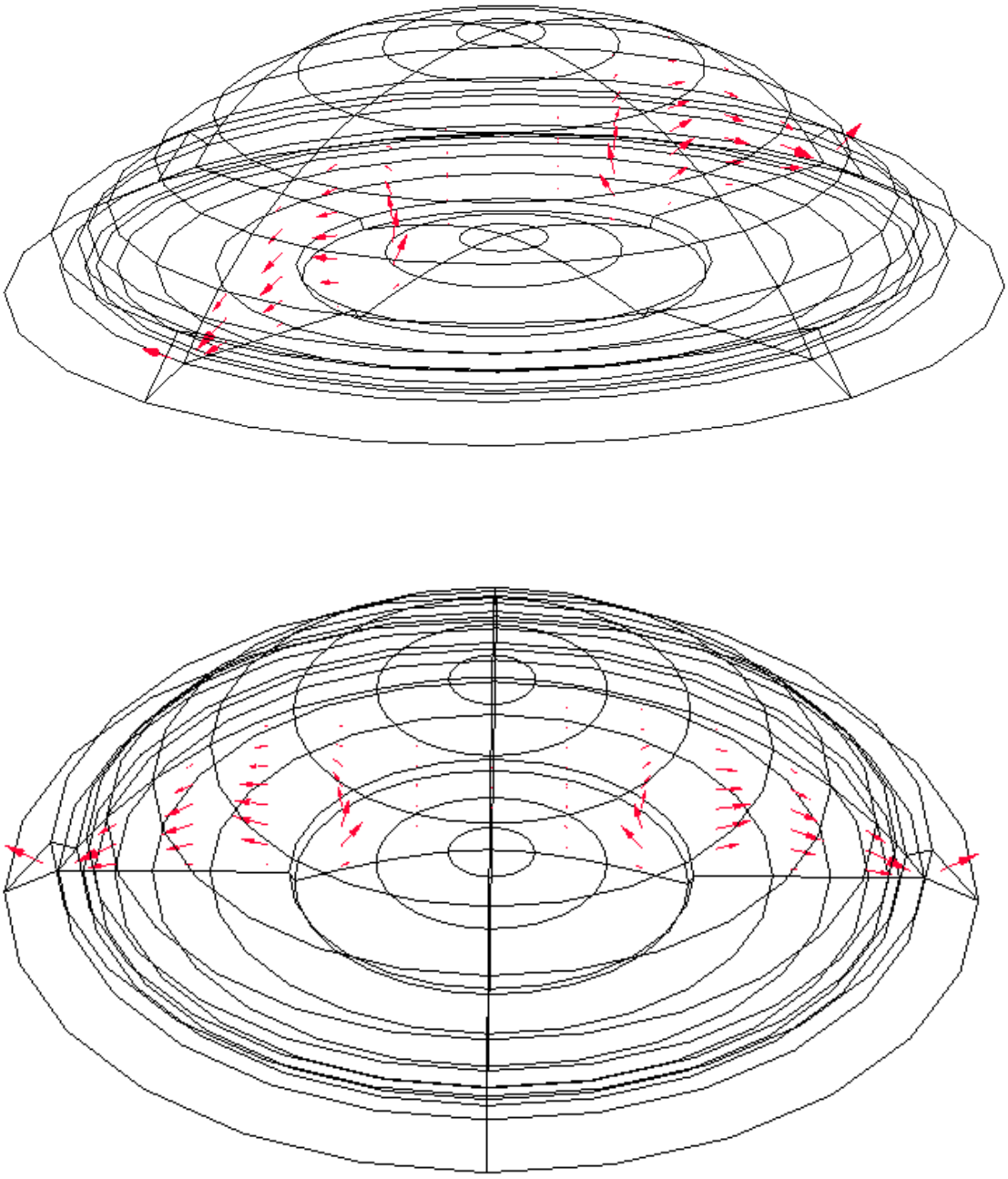

Figure 3.6. The cross section of the AH flow predicted by the 3D model in different perspective.

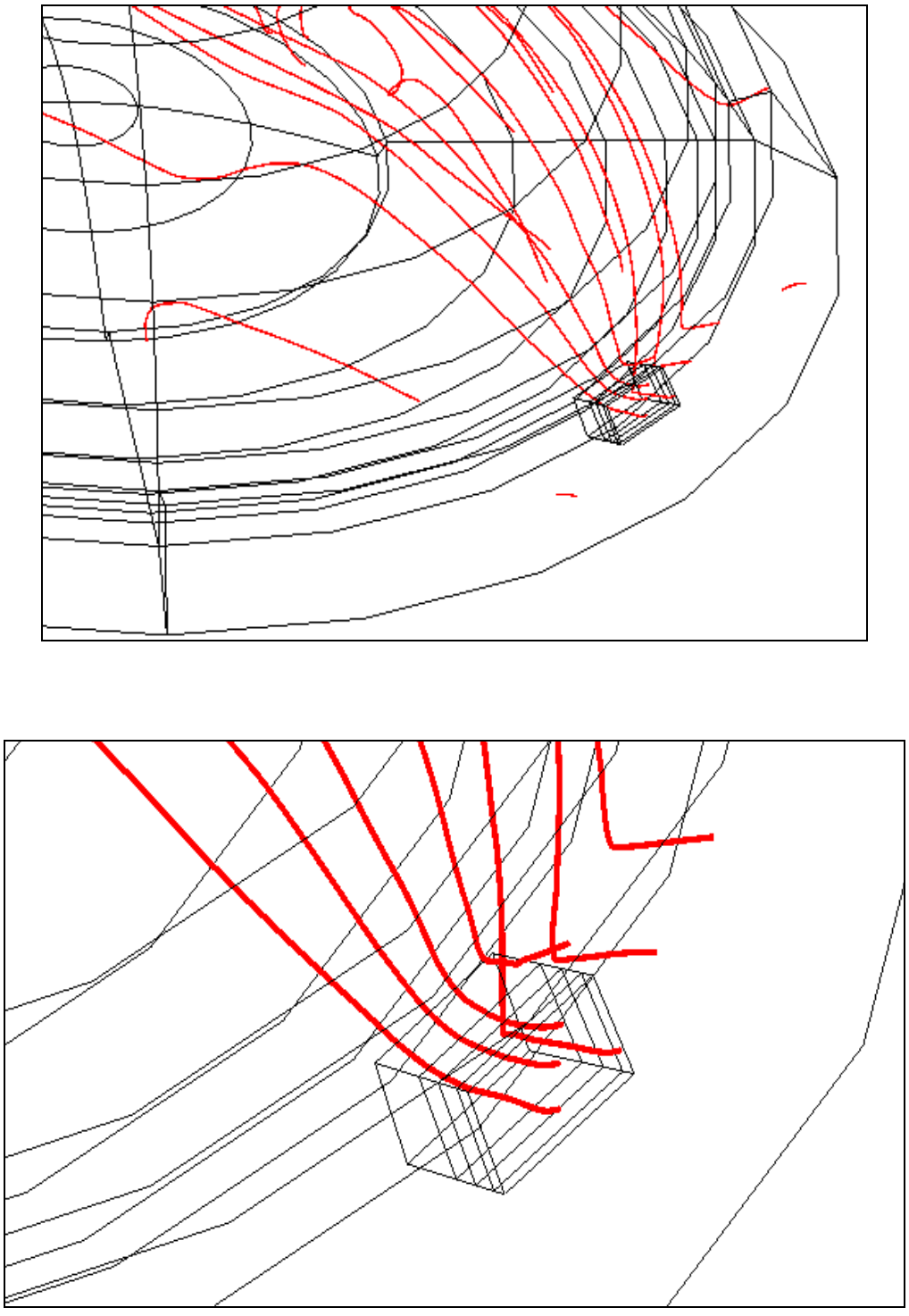

Figure 3.7. The flow through the channel seen in different perspective as predicted by the 3D model.

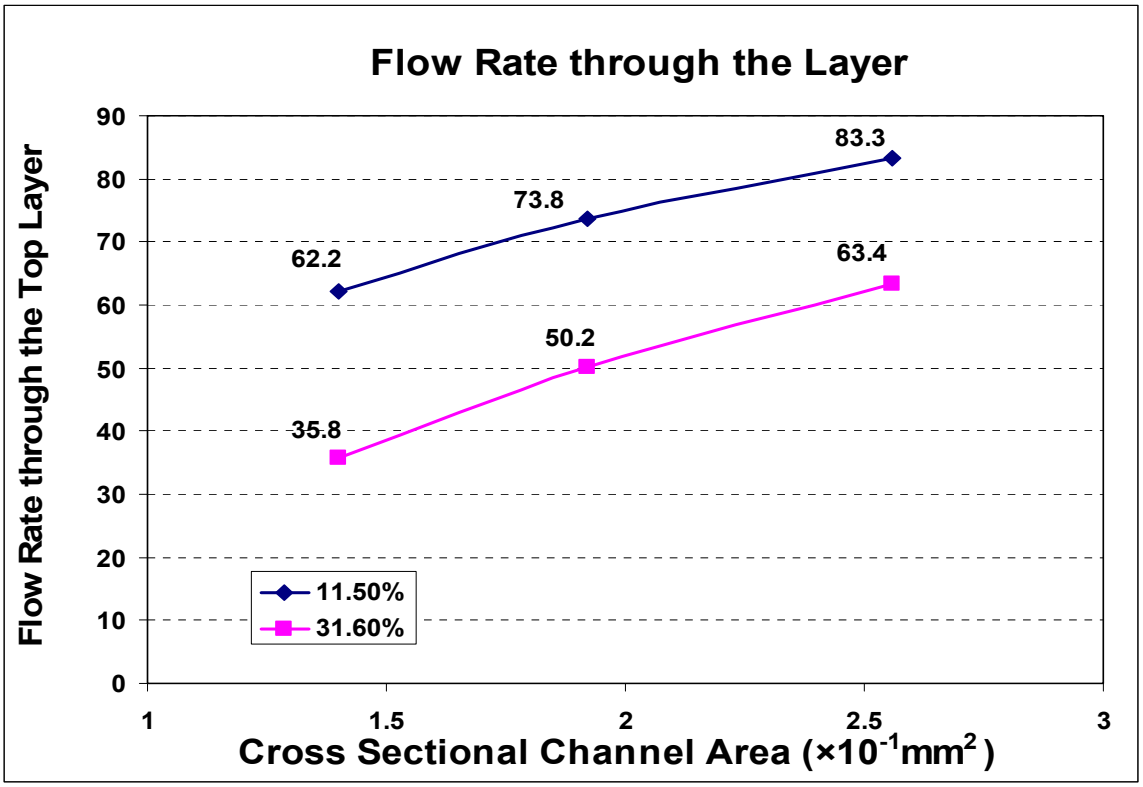

Figure 3.8. The flow rate through the remaining top layer of the channels as a function of the channel dimensions when thickness of the top layer is 11.5% of the toteal scleral thickness (blue diamonds) and 31.6% of the total thickness (red squares) respectively.

3.9. References

[1] E. C. Huang and V. H. Barocas, "Accommodative microfluctuations and iris contour," *Journal of Vision*, vol. 6, pp. 653-660, 2006.

[2] S. Kumar, S. Acharva, R. Beuerman, and A. Palkama, "Numerical solution of ocular fluid dynamics in a rabbit eye: Parametric effects," *Annals of Biomedical Engineering*, vol. 34, pp. 530-544, 2006.

[3] V. H. Barocas and J. J. Heys, "Computer simulation of passive iris deformation during blinking and accommodation," *Investigative Ophthalmology & Visual Science*, vol. 42, pp. 3563 Suppl. S, 2001.

[4] C. W. Lin, Y. Wang, P. Challa, D. L. Epstein, and F. Yuan, "Transslceral diffusion of ethacrynic acid and sodium flourescein," *Molecular Vision*, vol. 13, pp. 243-251, 2007.

[5] S. M. Podos and M. Yanoff, *Textbook of ophthalmology*. Philadelphia, PA: Gower Medical Publishers, 1994.

[6] I. Grierson, S. Nagasubramanian, J. Edwards, L. C. Millar, and K. Ennis, "The effects of vitreous level of intraocular pressure on the rabbits outflow system," *Experimental Eye Research*, vol. 42, pp. 383- 397, 1986.

[7] D. M. Silver and H. A. Quigley, "Aqueous flow through iris-lens channel: Estimates of differential pressure between the anterior can posterior chambers," *Journal of Glaucoma*, vol. 13, pp. 100-107, 2004.

[8] J. Sokol, Z. Stegman, J. M. Liebmann, and R. Ritch, "Location of the iris insertion in pigment dispersion syndrome," *Ophthalomology,* vol. 103, pp. 289-293, 1996.

[9] www.comsol.com/support

[10] H. A. Reitsamer and J. W. Kiel, "A rabbit model to study orbital venous pressure. Intraocular pressure, and ocular hemodynamics simultaneously," *Invest Investigative Ophthalmology & Visual Science*, vol. 43, pp. 3728-3734, 2002.

[11] J. H. Prince, *Rabbit eye in eye Research*. Springfield, IL: Charles. C. Thomas, 1964.

[12] Z. Y. Chen and C. M. Shao, "Evaluation of minimum factor of safety in slope stability analysis," *Canadian Geotechnical Journal*, vol. 25, pp. 735-748,1988.

[13] R. Ardito, G. Cocchetti, and G. Maier, "On structural safety assessment by load factor maximization in piecewise linear plasticity," *European Journal of Mechanics A-Solids*. vol. 27, pp.859-881, 2008.

CHAPTER 4

IN VIVO EXPERIMENT TO DEMONSTRATE THE POTENTIAL FOR CLINICAL STUDY

4.1. Introduction

It was demonstrated in Chapter 2 that a femtosecond laser created subsurface scleral channel in *ex vivo* rabbit eye increases the AH outflow leading to the IOP reduction. However, this was only qualitative assessment of the feasibility of IOP reduction by subsurface scleral channel, since the elevated IOP was mimicked by increasing the inflow into the anterior chamber and the effect was demonstrated by the increased outflow. Therefore, it is necessary to show the effect of subsurface scleral channels on the IOP under *in vivo* condition to demonstrate the actual effect that can be expected in the clinical study. It is also necessary to refine the experimental setup, because the scanning under *in vivo* condition can not be made by moving the object as it was possible in the *ex vivo* experiment.

In this chapter, the refined experimental setup will be shown to make scan by moving the focus. It will be assessed if the subsurface scleral channel can be created in

the eyes of *in vivo* rabbits as in *ex vivo* experiment. The effect of channel will be evaluated in the way that it is actually evaluated in the clinic. The important consequences will be discussed for the analysis of the results from *in vivo* experiment.

4.2. Methods

4.2.1. Experimental Setup

The laser delivery system introduced in Chapter 2 was used in this experiment. The scanning mechanism was altered to move the beam focus to scan the femtosecond laser pulses into the eye of *in vivo* rabbits as described in Figure 4.1 to Figure 4.2. Comprehensive scanning experiment was setup as shown in Figure 4.1. The rabbit holder was mounted on an adjustable stage so that the eye could be targeted at the optimal position for the laser treatment. A microscope slide was placed on the top of the eye by the means of a slide holder, avoiding the pressure on the eye, so that scattering at the scleral surface could be minimized. The laser beam was reflected by a mirror and propagated through the 0.5 NA focusing objective so that the focused beam passed down into the eye in normal direction to the surface of microscope slide as shown in Figure 4.1 and 4.2. The X, Y and Z axes were set up as described in Figure 4.2 in the same way as in Chapter 2. The difference from ex vivo experiment setup is that the aspheric lens was attached to the stage, as shown in Figure 4.2 controlled by the computer so that the focus can be moved in the predetermined pattern as shown in Chapter 2.

4.2.2. Experimental Procedure

New Zealand albino rabbit was anesthetized with ketamine and xylazine. IOP was measured 10 times with tonopen (Reichert Analytical Instrument; Depew, NY). Rabbit

was fixed in the holder, as shown in Figure 4.1 and the eye was located at the optimal position so that the limbus was on the propagation axis of laser beam. The microscope slide was placed on the eye where the channel needed to be created, maintaining the surface normal to the propagation axis of laser beam.

The position of the focusing lens was adjusted along Z axis so that the focus of laser beam was located at the angle of the eye as marked by red arrow in Figure 4.3. The focusing lens was located inside the expanded laser beam so that it could keep focused with irradiance higher than optical breakdown threshold for sclera during whole scanning process. The energy of laser beam was set to be 18 μJ. Scanning parameters were set to be a 2 μm spot separation, a 4 μm line separation and a 2 μm layer separation. The scanning was made in the same way as in *ex vivo* experiment introduced in Chapter 2 except that the lens was moved.

IOP values were measured 10 times after the laser treatment to evaluate the IOP reducing effect of channel. After the IOP measurement, the shape of channel was monitored with OCT image as shown in Figure 4.4 [1] to evaluate the efficiency of channel creation. Mean value over 10 measurements was used to evaluate IOP changes.

4.3. Results

One channel was created in each of four rabbits at the angle of the eye through the trabecular pathway as shown in OCT images of Figure 4.4 [1]. Dimensions of channel, width × length, were 450μm × 150μm, 600μm ×200μm, 600μm × 220μm and 800μm × 240μm, corresponding to cross sectional areas of 0.068, 0.12, 0.132 and 0.192

mm^2. As shown in Figure 4.4, the channel was created, remaining the thin layer between the top of channel and the anterior surface of sclera.

The channel in the eye imaged by the confocal microscope (see Figure 4.5) was scanned with the same parameters as the eye shown in Figure 4.4. It can be seen in Figure 4.5 that the thin layer on the top of the channel remained intact in the same way as in the eye shown on the OCT image in Figure 4.4, but the shape of channel is different from that shown in Figure 4.4. This difference is believed to be from the postmortem change in the sclera to be addressed in discussion section.

The effect of channel can be evaluated by the amount of reduced IOP, the difference in IOP values measured before and after the laser treatment. Figure 4.6 shows pre-treatment IOP value and the amount of reduced IOP over different channel dimensions. However, the amount of IOP reduction is affected by pre-treatment IOP value, because higher IOP induces higher outflow rate increase through channel, leading to higher levels of IOP reduction.

Therefore, the IOP reduction was normalized by the pre-treatment IOP value for the comprehensive evaluation of the channel effect as shown in Figure 4.7. It can be seen that the percentage based IOP reducing effect increases over the dimension of channel in a positive relation from 15 % to 48 %, indicating that the channel dimension has the dominant effect.

4.4. Discussion

The goal of this experiment was to demonstrate that the subsurface scleral channel with IOP reducing effect can be created in the eyes of *in vivo* rabbits. In the *ex*

vivo experiment described in Chapter 2, the effect of channel was demonstrated by the post-treatment outflow rate increased up to three to four times of the pre-treatment outflow because the experimental setup was designed to mimic the elevated IOP in glaucomatous eye so that the maximum amount of AH would flow through the remaining layer between the surface of sclera and the top of channel. Since the pressure in the eye was maintained by connecting the pressurized water reservoir to the eye, IOP reduction cannot be demonstrated in the perfusion experiments.

In addition to this, it is also obvious in Figure 4.7 that the IOP reduction of channel has a positive relation with dimensions of channel, proposing the strong potential of controlling the IOP reduction by adjusting channel dimensions. Therefore, it can be concluded that the disadvantages of current glaucoma treatment, such as infection and difficulty in controlling the value of post-treatment IOP, may be significantly improved with the femtosecond klaser treatments. The limited longevity of usage, the major disadvantage of LT, is expected to be reduced also, because it is expected that the effect of subscleral channel would last longer than scratch or widened hole by LT.

The shape of channel before and after the sacrifice of a rabbit can be reconstructed with lines based on Figure 4.4 and 4.5 as shown in Figure 4.8. The channel shape in Figure 4.4 can be explained by the existence of force by IOP, red arrows in Figure 4.8(a). The channel shape in Figure 4.5 can be reconstructed as Figure 4.8(b). The difference in the shape of channel can be explained by the postmortem change in the sclera and the absence of IOP. As it was mentioned in Chapter 1, the sclera maintains the shape of the eye with its rigidity [2], indicating that the balance

between the sclera rigidity and IOP maintains the shape of the eye. Under *in vivo* condition, the channel is created in the existence of IOP. Therefore, once the channel is created, the IOP inside the channel maintains the shape of channel as described in Figure 4.8 (a).

However, IOP is reduced significantly and the rigidity of sclera is changed after the rabbit is sacrificed. In addition to this, the rigidity and the force on sclera by IOP can not be uniform over the sclera, indicating the possible different postmortem changes depending on the position in the sclera. This also demonstrates the advantage of monitoring the shape of channel by OCT that can show the intact shape of channel under *in vivo* condition.

IOP was measured by the commercial tonopen (Reichert Analytical Instruments; Depew, NY). Tonopen is so reliable as it is used in clinic [3] and IOP values measured in this study is also reliable. Therefore, it can be concluded that it is very likely that this IOP reducing result can be achieved in the clinical study also.

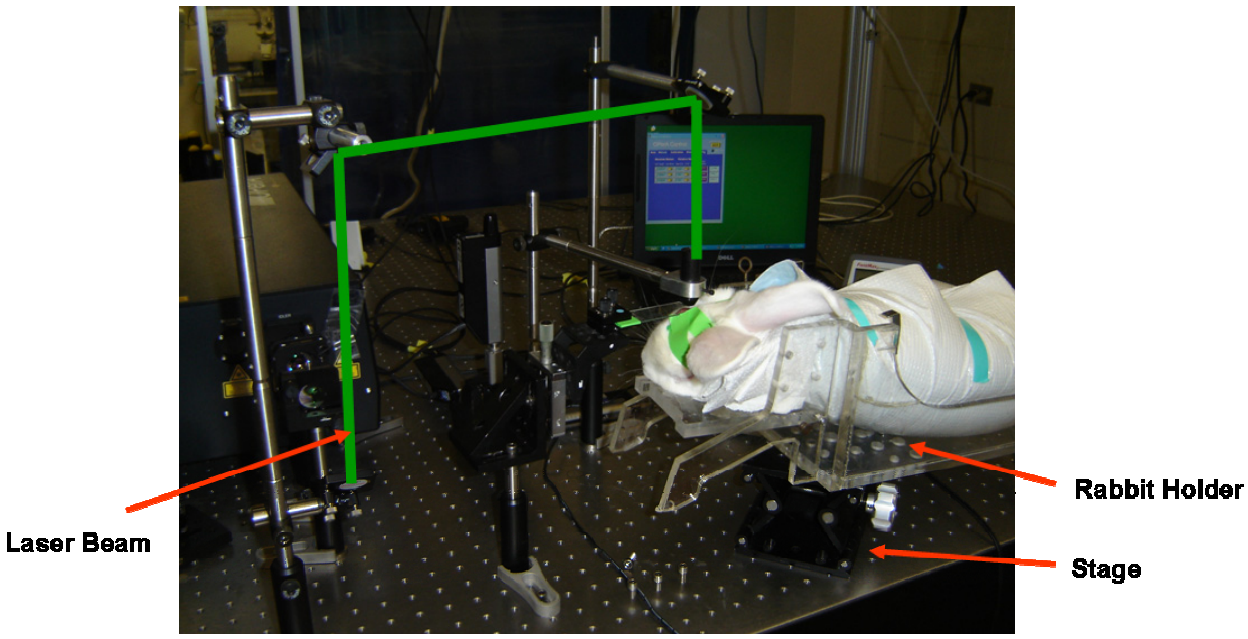

Figure 4.1. The experimental setup to scan the femtosecond laser beam into the eye of a live rabbit.

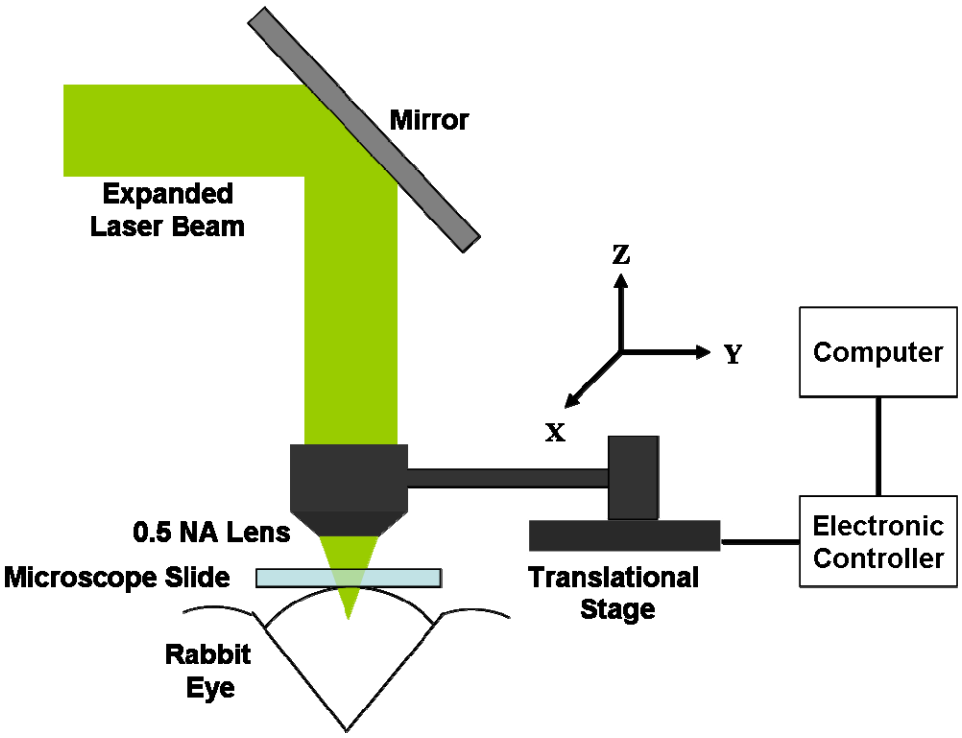

Figure 4.2. The scanning mechanism for *in vivo* experiment.

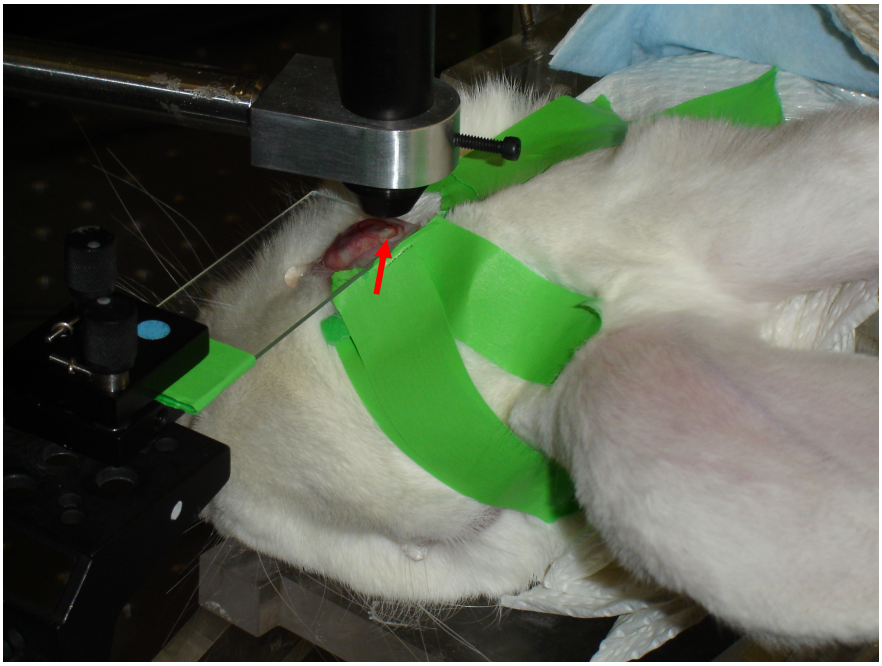

Figure 4.3. Setting up the starting position of scanning.

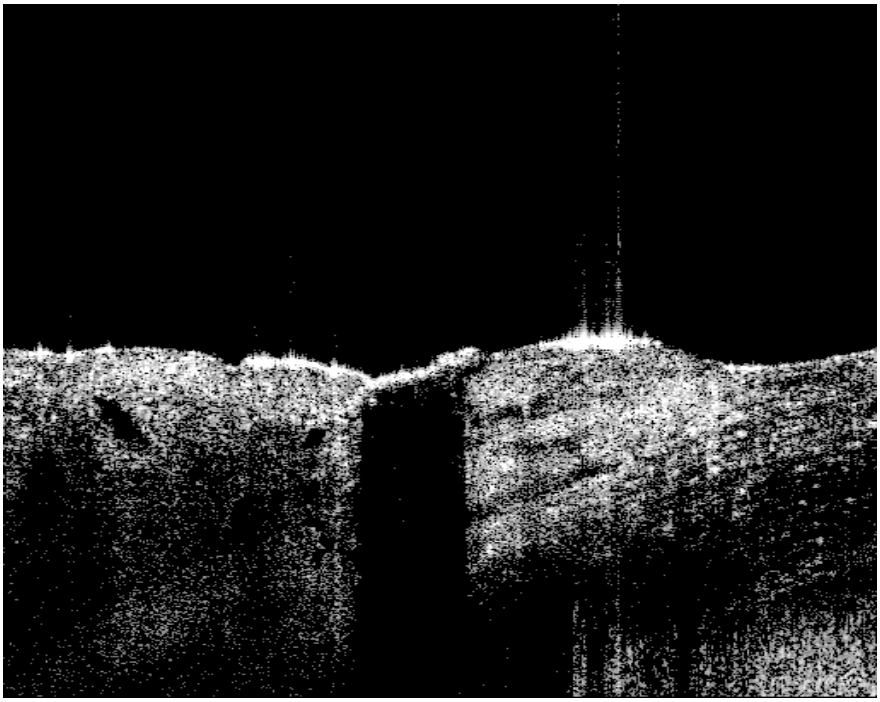

Figure 4.4. OCT image of subscleral drainage channel created by scanning [1].

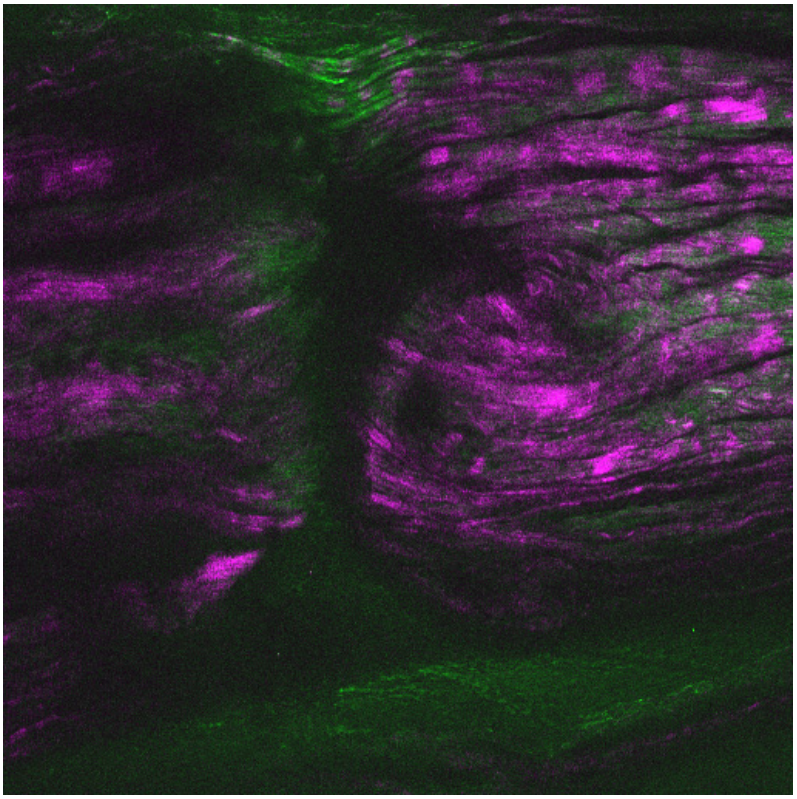

Figure 4.5. Confocal microscope image of channel.

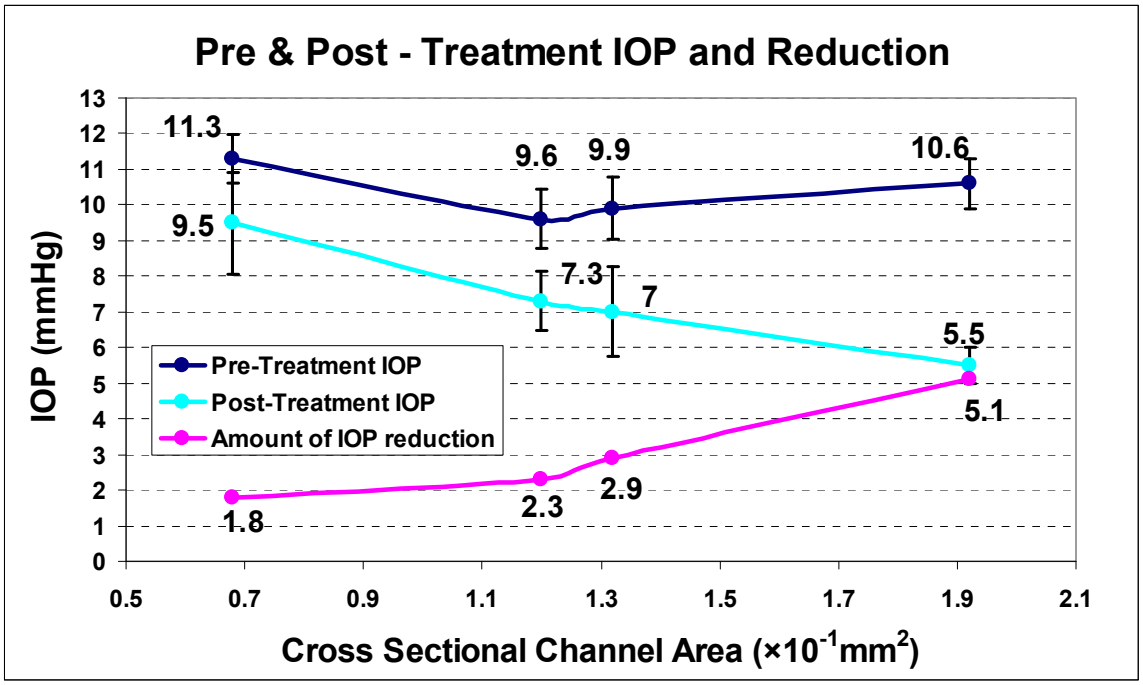

Figure 4.6. IOP values to be considered in the evaluation of channel effect in each channel.

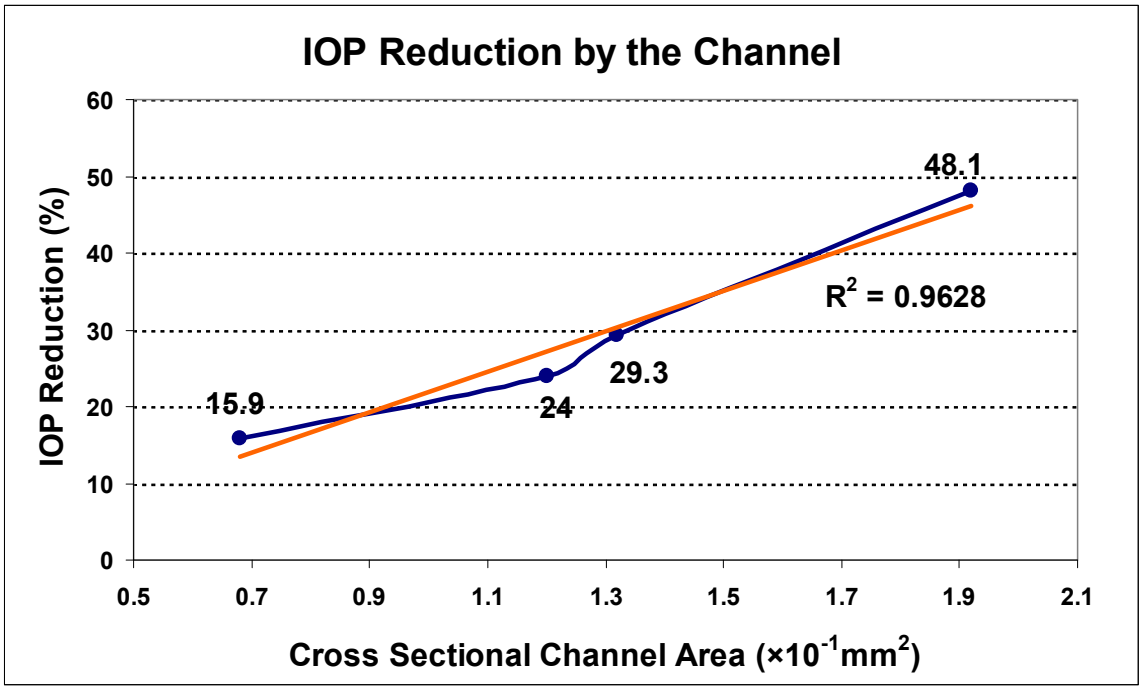

Figure 4.7. The normalized effect of IOP reduction as the function of channel dimension.

.

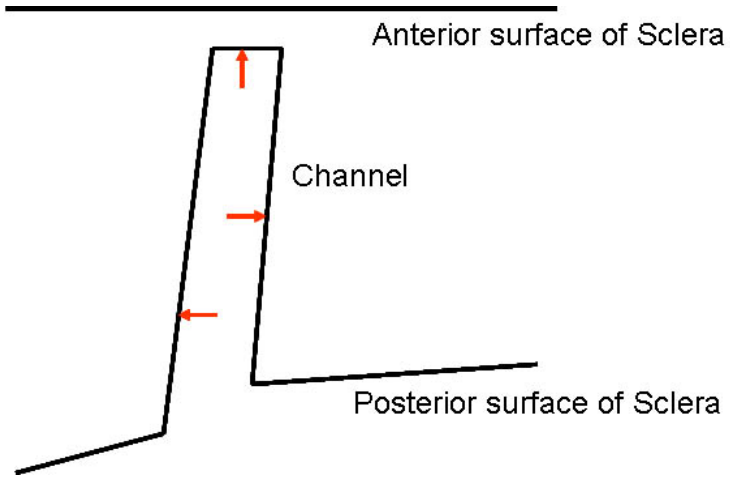

(a)

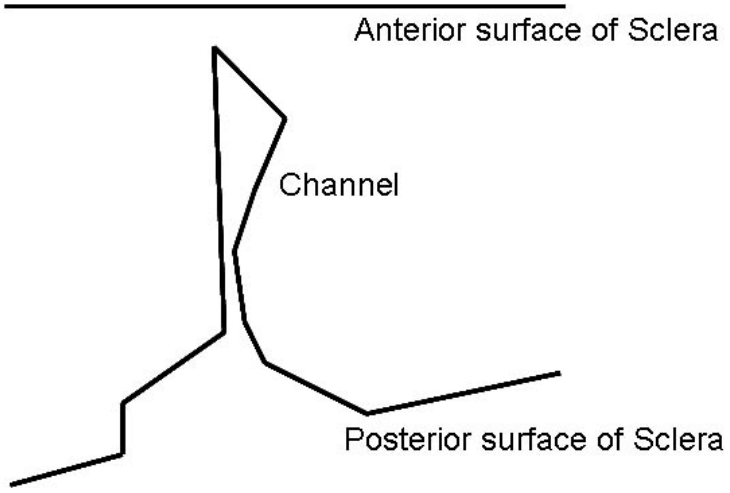

(b)

Figure 4.8. The shape of channel before and after the sacrifice ((a) Predicted channel shape under *in vivo* condition based on OCT image with red arrowed IOP, (b) Distorted channel shape due to the postmortem changes in ocular tissues).

4.5. References

[1] G. Chaudhary, *Visualization assisted high-precision ophthalmic micro-surgery with femtosecond laser*. Ph.D dissertation. The University of California, Irvine.

[2] P. G. Watson and R. D. Young, "Scleral structure, organization and disease. A review," *Experimental Eye Research*. vol. 78, pp. 609-623, 2004.

[3] J. C. Morrison and I. P. Pollack, *Glaucoma: Science and Practice*. New York: Thieme Medical Publishers, 2003.

CHAPTER 5

CONCLUSIONS AND FUTURE STUDIES

5.1. Summaries and Contribution of Dissertation

Since advantageous properties of a femtosecond laser were found, various potential applications of femtosecond laser pulses have been proposed. The work in this dissertation materialized the non-invasive surgical procedure significantly reducing the disadvantages limiting the efficiency of currently used treatments. Additionally, the potential of a tool supporting the procedure was proposed. The contribution of the works in this dissertation can be summarized by each chapter like the following:

In Chapter 2, the experiment was conducted on *ex vivo* rabbit to create the subsurface scleral channel as a first step to assess the feasibility of potential of a subscleral channel as a treatment for glaucoma. The contribution made by this experimental work can be listed as following;

1. The demonstration of the feasibility that the subsurface scleral channel can be created with femtosecond pulses in the eye through the trabecular pathway.
2. The demonstration of AH outflow increasing effect of channel that can be controlled by adjusting the dimensions of channel.

3. The demonstration of advantageous property of treatment by a femtsecond laser that can leave the surface sclera intact without any damage to the neighboring tissues inducing scar and infection.

In Chapter 3, 3D finite element model was developed. The goal of glaucoma treatment is to continuously manage IOP within the normal range and a tool that can predict IOP is needed to determine the details of treatment such as dimensions and location of channel. The modeling work contributed to demonstrating the potential of the following:

1. 3D FEM model to predict the reduced IOP and propose the optimal treatment.
2. The new methodology to quantify the effect of the channel by the permeability of the remaining layer.

In Chapter 4, the experiment was performed on the eyes of in *vivo* rabbits to create the channels in different dimensions. It was demonstrated that the subsurface channel could be created with the altered experimental setup by moving the focus to make a scan. This *in vivo* experimental study made the following contributions:

1. The demonstration of the creation of subsurface channel by a femtosecond pulse and its IOP reducing effect under in vivo condition very similar to the clinical study.
2. The proposition of the strong potential that the reduced IOP can be controlled under *in vivo* condition.
3. The proof of the effect of postmortem change in scleral tissue on the shape of channel. This result will provide the valuable guide for the analysis of

experimental result, taking into account the postmortem change and the prediction of *in vivo* result from *ex vivo* experiment.

5.2. List of Publications

The following contributions were made during the works for this dissertation.

1. D. Chai, G. Chaudhary, R. M. Kurtz, and T. Juhasz, "Aqueous humor outflow effects of partial thickness channel in *ex vivo* eyes," *Proceedings of SPIE,* vol. 6426, pp. 64350O, 2007.
2. D. Chai, G. Chaudhary, E. Mikula, H. Sun, and T. Juhasz, "3D finite element model of aqueous humor to predict the effect of femtosecond laser created partial thickness channels on the IOP," ASLMS: *American Society for Laser Medicine and Surgery*, Grapevine, Texas, April 2007.
3. D. Chai, G. Chaudhary, E. Mikula, H. Sun, and T. Juhasz, "Modeling the effect of femtosecond laser created intrascleral channel in rabbit eye," ARVO: *The Association for Research in Vision and Ophthalmology*, Fort Lauderdale, Florida, May 6-10, 2007.
4. D. Chai, G. Chaudhary, E. Mikula, H. Sun, R. M. Kurtz, and T. Juhasz, "*In vivo* creation of subscleral channel in rabbit eye with femtosecond laser". ARVO: *The Association for Research in Vision and Ophthalmology*, Fort Lauderdale, Florida, April 27 - May1, 2008.
5. D. Chai, G. Chaudhary, E. Mikula, H. Sun, and T. Juhasz, "3D finite element model of aqueous outflow response to femtosecond laser glaucoma treatments," *Lasers in Surgery and Medicine*, vol. 40, pp. 188-195, 2008.

6. D. Chai, Chaudhary. G, Mikula. E, Sun. H, R. Rurtz, and Juhasz. T, "IOP reduction after femtosecond laser subsurface scleral treatments in the eyes of in vivo rabbits," submitted to *Journal of Glaucoma*, 2008.

5.3. Direction of Future Studies

5.3.1. The Refinement of the Experimental Setup for the Creation of Channel through the Trabecular Pathway

Figure 5.1 and 5.2 show the procedural differences between cornea treatment and sclera treatment. It can be seen that a more refined experimental setup that can move and rotate the head to locate the eye at the proper angle for the treatment is needed for treatment through the sclera. As described in Figure 5.1, the cornea treatment does not use detailed positioning equipment due to the following reasons: 1) cornea is transparent and most protruding part of the eye, 2) the methodology of cornea treatment is to create a flap by making a cut in the cornea. However, as described in Figure 5.2, the equipment for detailed positioning is needed in the channel creating laser treatment through sclera in this study for the following reasons: 1) the sclera is translucent, 2) the channel is created by scanning the eye from the bottom of the translucent sclera and through the designated route, the trabecular pathway. Figure 5.3 shows that, even though scanning begins at the same position, channels with different effects can be created depending on the angle of the beam. Therefore, an experiment setup that can adjust the position and angle of the eye is needed for more advanced treatment with consistent success.

5.3.2. The Equipment for more Effective and Exact Evaluation of Treatment

The channels created in this study are subsurface ones and the shape, dimension and location of channel are critical. Therefore, efficient monitoring of the intact channel is essential to determine the optimal treatment procedure. Image of intact channel under *in vivo* condition can not be obtained with the conventional microscope image, because the damages to tissues, causing the changes of shape and location of channel, are unavoidable during the processes, such as cutting and fixation, for microscope imaging. Therefore, OCT was used in this study for imaging of the channel as it was created under *in vivo* condition. However, as described in Figure. 5.4, even when using OCT equipment is needed to locate the eye in the position such that the exact dimension, shape, and location of channel can be imaged by OCT at the consistent angle to the scanning direction.

5.3.3. The Optimization of Procedure by the Real-Time Monitoring

Even though the experimental study on the eyes of the *in vivo* rabbit was successful in this study, the procedure can be optimized by adjusting the scanning parameters, beam energy, and starting and ending the scanning the exactly projected positions. Then, IOP will be able to be reduced with minimal tissue damage, reducing IOP as much as needed. It is most significant to locate the focal point of beam at the projected position in the sclera. It cannot be completed with the refined setup mentioned in section 5.2.1, as shown in Figure 5.5, because the actual position of focus can not be monitored, even though it could be set up at the proper angle. Therefore, the real time monitoring system is needed to start the scan at the projected position. Then, the energy of the beam can be determined so that it will be slightly higher than the threshold of

LIOB. Finally, the scanning can be stopped exactly at the predetermined end position leaving a layer with the projected thickness.

It should be a long term goal to monitor in real time what happens in the sclera. Considering the channel is created with laser scanning, OCT has the potential to be intuitively incorporated into the existing laser delivery housing, eliminating the need for a stand-alone imaging probe.

5.3.4. **The Effect of Wound Healing on the Longevity of Treatment**

Once the channel is created in the eye of the living animal, it is supposed to be healed by the physiological wound healing. Following the wound healing process, it is expected that the space of channel will be filled over time, as described in Figure 5.6, and the IOP reducing effect of channel will be reduced also. Therefore, it is necessary to monitor the wound healing process over time to evaluate the longevity of the treatment and, ultimately, develop a follow up treatment that can maintain the IOP reducing effect of channel as long as needed.

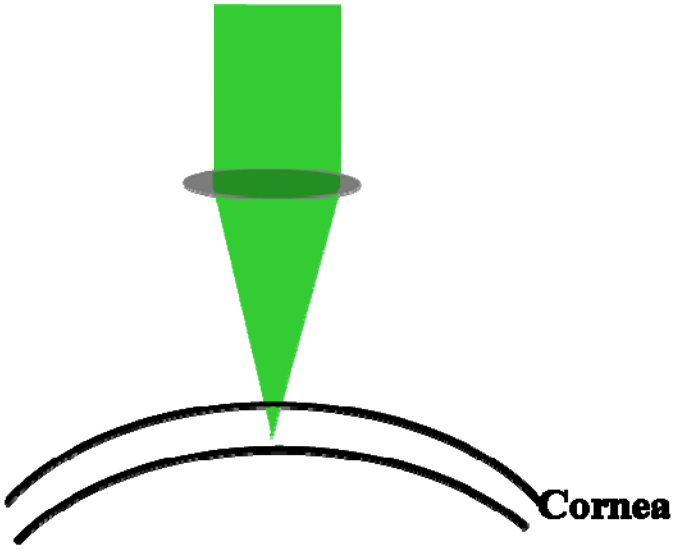

Figure 5.1. Scheme of the laser treatment on cornea.

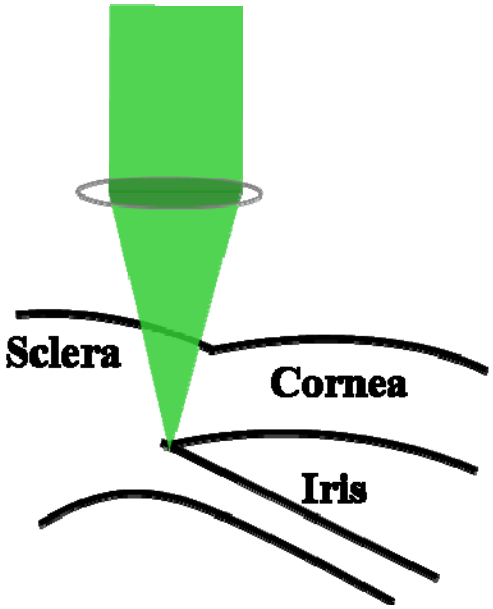

Figure 5.2. Scheme of the laser treatment through trabecular meshwork.

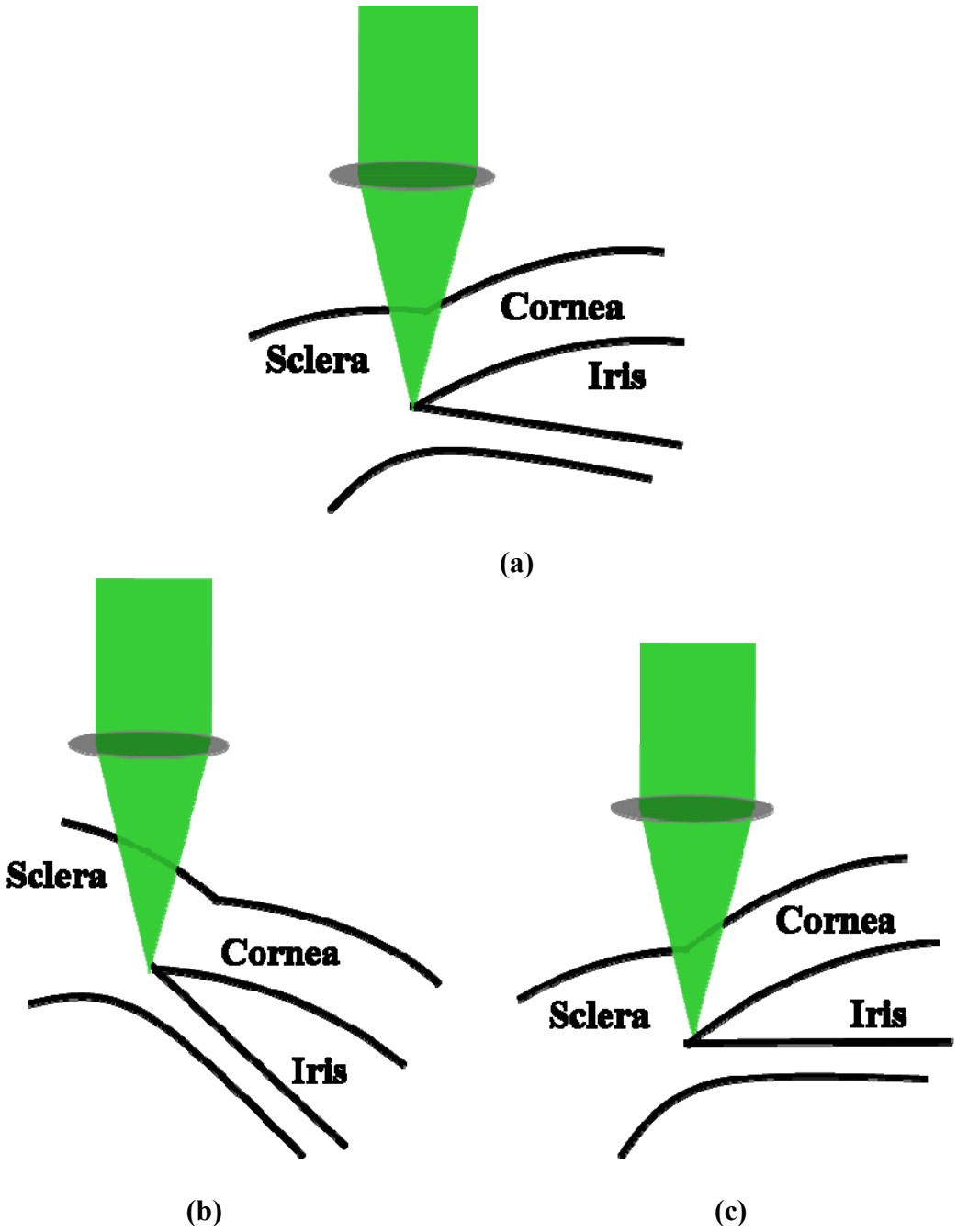

Figure 5.3. The cases of positioning ((a) Right angle, (b) Overrotated and (c) Underrotated).

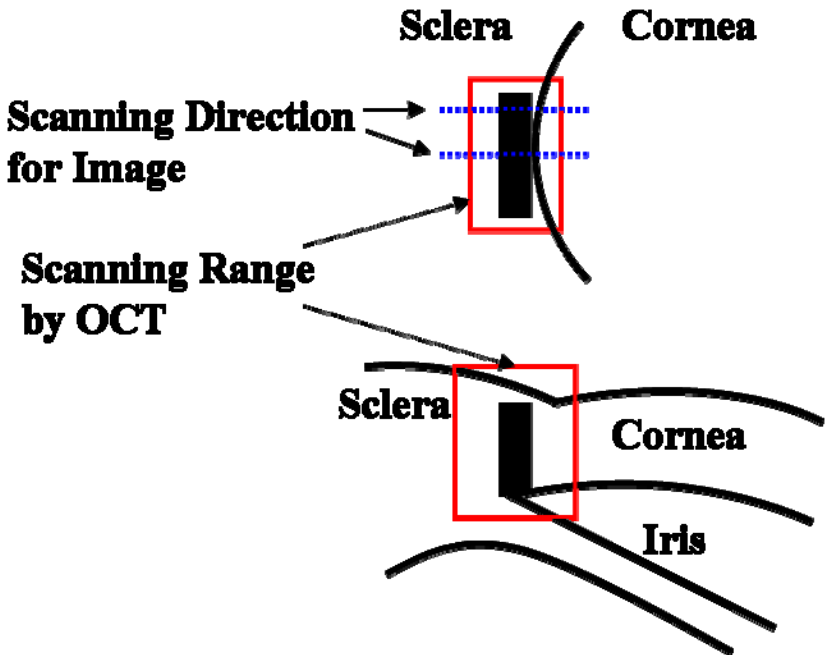

Figure 5.4. Scheme of OCT scanning.

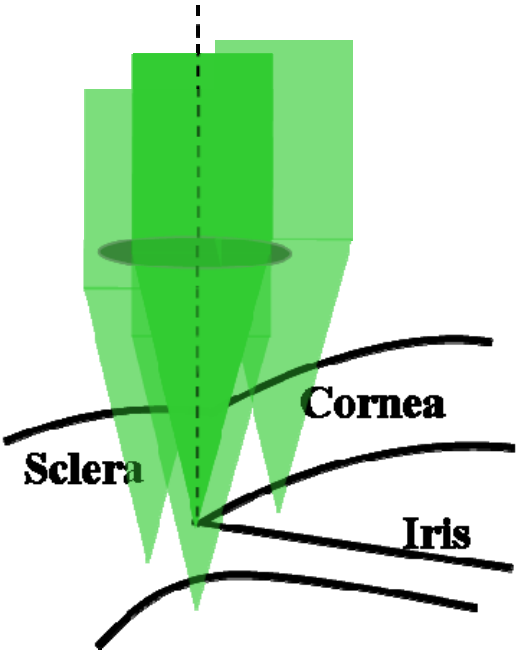

Figure 5.5. Different scanning at the same angle depending on the starting positions.

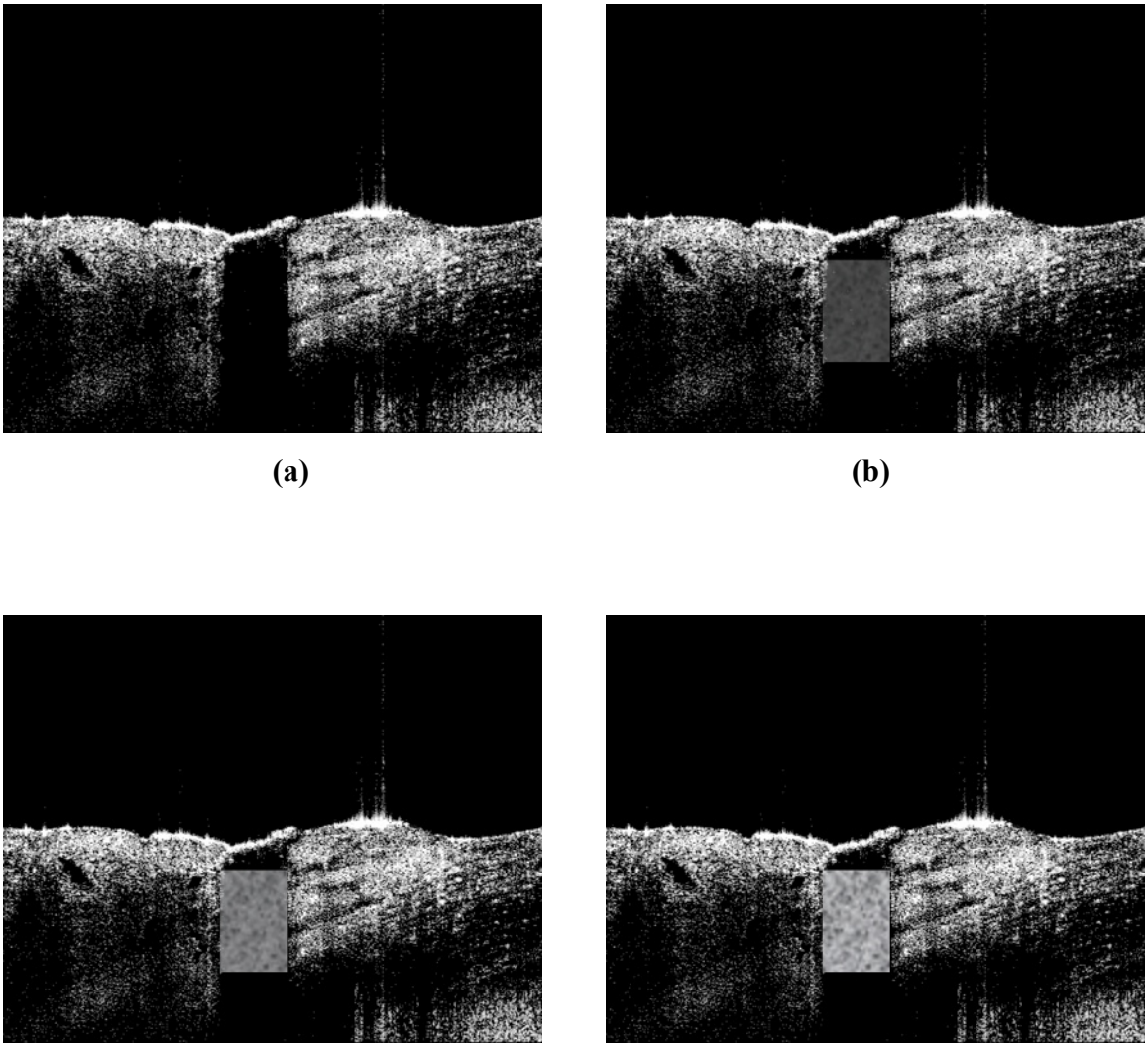

Figure 5.6. The expected wound healing process over time from (a) intact channel to (b), (c) and (d) healed channel over time.